4-14-2016 12:00 AM

Sensorless Rotor Position Estimation For Brushless DC Motors

Iram G. Raza
The University of Western Ontario

Supervisor
Lyndon J. Brown
The University of Western Ontario

Graduate Program in Electrical and Computer Engineering
A thesis submitted in partial fulfillment of the requirements for the degree in Master of Engineering Science
© Iram G. Raza 2016

Abstract

Brushless DC motor speed is controlled by synchronizing the stator coil current with rotor position in order to acquire an accurate alignment of stator rotating field with rotor permanent-magnet field for efficient transfer of energy. In order to accomplish this goal, a motor shaft is instantly tracked by using rotating rotor position sensors such as Hall effect sensors, optical encoders and resolvers etc. Adding sensors to detect rotor position affects the overall reliabiltity and mechanical robustness of the system. Therefore, a whole new trend of replacing position sensors with sensorless rotor position estimation techiques has a promising demand.

Among the sensorless approaches, Back-EMF measurement and high frequency signal injection are the most common. Back-EMF is an electromotive force, directly proportional to the speed of rotor revolutions per second, the greater the speed motor acquires the greater the Back-EMF amplitude appears against the motion of rotation. However, the detected Back-EMF is zero at start-up and does not provide motor speed information at this instant. Therefore, Back-EMF based techniques are highly unfavourable for low speed application specially near zero. On the other hand, signal injection techniques are comparatively developed for low or near zero motor speed applications and etimate on-line motor parameters exploiting identification theory on phase voltages and currents signals.

The signal injection approach requires expensive additional hardware to inject high frequency signal. Since, motors are typically driven with pulse width modulation techniques, high frequency signals are naturally already present which can be used to detect position. This thesis presents rotor position estimation by measuring the voltage and current signals and also proposes an equivalent permanent-magnet synchronous motor model by fitting the data to a position dependent circuit model.

Keywords: BLDC motor position, Rotor position, Sensorless control of BLDC motor, Rotor position identification, Back-EMF, Commutation, Initial posistion estimation, signal injection.

Acknowledgment

I want to acknowledge my profound gratitude and appreciation to my honourable supervisor, **Dr. Lyndon J. Brown**, Associate Professor, Department of Electrical and Computer Engineering, Western University, Canada, for his utmost help, guidance, step by step exhortation towards improving research and sagacious supervision all through my study and research, during my M.E.Sc program.

My earnest regards to my dear department teachers who enhanced my knowledge and offered their support and encouragement. I would also like to thank ECE graduate staff my fellow graduate research understudies and specialized assitance from ECE designing workshop and writing support services.

Last but not the least, I cannot ignore a token of appreciation to my family and companions for their undeviating love, support and motivation. I would also want to express my gratitude to my friends for their innovative and constructive suggestions and discussions.

Contents

List of Figures

List of Tables

List of Appendices

List of Acronyms

ADC: Analogue to digital convertor
AFPM: Axial flux permanent-magnet
ANFIS: Adaptive network based fuzzy interference system
BACM: Brushless AC motor
BDCM/BLDC: Brushless DC motor
DC: Direct current
DQO: Direct quadrature and zero
DSP: Digital signal processing
DTC: Direct torque control
DUT: Device under test
ECBM: Electronically commuted brushless motor
ECDCM: Electronically commuted DC motor
EKF: Enhanced Kalman filter
EMF: Electromotive force
EEMF: Extended EMF
EVs: Electric vehicles
FFT: Fast Fourier transform
FOC: Field oriented control
FPGA: Field programmable gate array
IM: Induction motor
IMP: Internal model principle
IPMSMs: Interior permanent magnet synchronous motors
LCR: Inductance(L), capacitance(C), and resistance(R)
LMS: Least mean square
LQR: Linear quadratic regulator
MIPS: Million instructions per second
MMF: Magnetomotive force
MPC: Model predictive control
MTPA: Maximum torque per ampere
PMBDC: Permanent-magnet brushless DC motor
PMSM: Permanent-magnet synchronous motor
PWM: Pulse width modulation
RLS: Recursive least sqaure
rpm: Revolutions per minute
RSW: Resistance spot weldding
SMO: Sliding mode observer
SPMSM: Surface PM synchronous motor
SRM: Switched reluctance motor

VR: Variable reluctance
ZCD: Zero-crossing detection

List of Symbols

a, b, c: Coefficeints of polynomials

A, B, C: Motor Phases

A_{11}, A_{12}, A_{21}:   EEMF state space matrices

A_c: Area of crossection of a conductor [m^2]

a_m, b_m: Tunning function design coefficients

A_m: Amplitude of sinusoidal wave for m=1,2,3,$\cdots$

B: *Magnetic field density* [Wb$\cdot m^{-2}$]

B_m: Amplitude of the offset of a signal, for $m = 1, 2, 3, \cdots$

BW: Bandwidth [Hz]

c_m: Chebyshev filter design coefficients, for $m = 1, 2, 3, \cdots$

$C(s)$:   Transfer function of controller

d/dt: derivation operator

dq: d-q coordinates on rotating frame

$D(s)$:   Characteristic function of T_{de}

e,e_α, e_β: EEMF at stationary frame reference [V]

E: Exponent

ε: EMF induced [V]

ε_i: Damping ratio

$\mathcal{F}$:   Magneto-motive Force [A$\cdot turns$]

G: PMSM Observer gain

H: Magnetic field strength [A$\cdot m^{-1}$]

$H(s)$:   EEMF filter transfer function

i: Current [A]

i: index number

I: Identity Matrix

I_A, I_B, I_C: Motor phase currents [A]

I(s):   Frequency response of current [A]

j: Complex number

J: $\frac{\pi}{2}$-degree rotation matrix with reference to I matrix

J_c: Cost function

J_m: Moment of inertia of motor [kg $\cdot$ m^2]

k: Number of samples

K_{1i}, K_{2i}:   IMP controller gain matrices

K_b: Induced EMF constant [V/(rad/s)]

K_e: Eddy current loss

K_f: Frictional constant

K_t: Torque constant [N $\cdot$ m/A]

l: Length of conductor [m]

L: Inductance [H]

L_{AB}:   Phase AB inductance [H]

L_{BC}:   Phase BC inductance [H]

L_{CA}:   Phase CA inductance [H]

L_{align}:   Inductance: for aligned poles [H]

L_{base}:   Off-set inductance [H]

L_{dev}:   Deviation in inductance [H]

L_0, L_1:   Average inductances of between L_d & L_q [H]

L_d: Direct Inductance [H]

L_q: Quadrature Inductance [H]

l_{g1}:   Airgap of yoke [mm]

l_{g2}:   Airgap between pole teeth [mm]

l_m: Thickness of magnet [mm]

L_{max}:   Maximum inductance [H]

L_{med}:   Intermediate Inductance [H]

L_{min}:   Minimum inductance [H]

$L(s)$:   Transfer function of tunning function in IMP algorithm

$L_{unaligned}$:   Inductance of unaligned poles [H]

M_i: Mutual inductance [H]

M_m: EEMF RLS estimation cofficients for m=1,2,3,$\cdots$

M(s):   *Numerator of transfer function L(s)*

μ_o: Permeability of free space [H$\cdot m^{-1}$]

μ_r: Permeability of material relative to free space [H$\cdot m^{-1}$]

N: *Total number of turns in winding*

N_s: Synchronous speed [rpm]

$N(s)$:   Dinominator of Transfer function L(s)

O: Null matrix

ρ: Derential operator, or d/dt

P: Number of rotor poles

Q_c, R_c: Correlation matrices

$Q(2\Delta\theta_{re})$:   Cosine matrix of rotation

R, R_1, R_2:   Resistance [Ω]

$\mathcal{R}$:   Reluctance [H^{-1}]

$\mathcal{R}_d$:   Direct axis relctance [H^{-1}]

R_m: Resistance of the magnetic circuit [Ω]

$\mathcal{R}_q$:   Quadrature axis relctance [H^{-1}]

R_s: Stator resistance [Ω] $S(2\Delta\theta_{re})$:   Sine matrix of rotation

s: Frequency doamin symbole for derivative

s(t):   Time varying sinosuidal signal input

T: Torque [N$\cdot m$]

T_{bpn}:   Transfer function of band pass notch bank

T_{de}:   Desired Transfer function for IMP controller

T_e: Electric torque [N·m]

T_L: Load torque [N·m]

ΔT_s: Sampling rate [$Samples/s$]

U: Input

U_{cos} , U_{sin}:   Resolver deriving sine and cosine voltages [V]

ω: Angular frequency [rad·sec^{-1}]

ω_i: i^{th} harmonic of the fundamental frequency [Hz]

ω_o: Fundamental frequency [Hz]

ω_r: Rotor speed [rad·sec^{-1}]

x_i, x_{mn}:   State variables for i,m,n=1,2,3,···

x^T: Transpose of the state variable matrix

z_p: Phase to phase equivalent impedance for RL-parallel model [Ω]

z_s: Phase to phase equivalent impedance for RL-series model [Ω]

$\alpha\beta$: $\alpha\beta$ coordinates on stationary frame

$\gamma\delta$:   Estimate co-ordinates on rotating frame

λ_s: Stator flux linkage [Wb·$turns$]

ϕ: Flux [Wb]

ψ: Flux linkage [Wb·$turns$]

θ_{re}:   Electrical angle   [rad]

θ_m: Mechanical angle   [rad]

θ_r: Rotor angle [rad]

Chapter 1

Background

1.1 Overview

Everyday increasing global warming and sky-rocketing fuel prices are promoting the manufacture of electric vehicles (EVs). Not until the mid 20th-century were numerous electric vehicles, e.g, lawn mowers, electric bikes, cars, wheelchairs and golf carts commercially introduced by several car companies. The earliest electric vehicle model was not solely an electric one, but was a hybrid that could be operated by both gasoline as well as an electric power generator. However, from the mid 20th-century until today many big vehicle companies have been in competition to introduce high performance and energy efficient electrical cars and other vehicles every year [1].

To enhance the battery time of EVs, the smallest number of electric power consuming components are required. For this purpose, electronically controlled brushless motors, such as switch reluctance motors (SRM), induction motors (IM) and permanent-magnet synchronous motors (PMSM) are preferred over brushed motors as they consume comparatively less average battery power. The permanent magnetic synchronous motors are recommended in high torque, better traction and low speed operation and because of their high magnetic power density (i.e, the amount of power per unit volume), ruggedness, high efficiency, reliability and field weakening torque control [2, 3].

1.2 Motivation

The main motivation to develop this thesis is to emphasize the current industrial requirement to replace rotor position sensors with sensorless approaches to improve the EVs' battery time, enhancing the overall performance and reliability of brushless DC motors.As sensors consume electric power and are mostly mounted on the rotor itself which are more prone to damages in rugged environmental conditions. A Sensorless rotor position technique require no external hardware i.e, sensors and connecting wires etc. Extracting rotor position information from its phase excitation signals, such as voltage and current, can improve the reliability of the entire system. Furthermore, rotor position dependent phase model development is required to interpret the actual PMS motor operation.

In torque and speed control of switch reluctance and permanent magnetic synchronous motors, rotor position is acquired using Hall effect sensors, optical encoders and resolvers etc. Utilization of external sensors with interfacing devices not only requires additional power consuming components, but also increases the maintenance cost. A whole new trend to remove the sensors to measure rotor position is emanating within the auto-mobile companies across the globe to enhance the reliability of EVs. Most of the ongoing research in this area is lacking a suitable, and equivalent rotor position sensing model. A rotor position dependent motor model can completely replace its position sensors which can especially benefit at the start-up and at slow-speeds region of motor operation.

The commutation is a process of continuous supply of voltage pulses to maintain the rotating field and permanent-magnet field alignment by designing a (ON cycle) pulse modulated signal. Commutation requires an instantaneous track of rotor position (mostly with sensors) to maintain a consistent speed and for a swift transition of motor speed to other reference levels with least impact to the cogging effect in motor torque. Another explanation for providing voltage pulses to each phase with proper frequency and angle is as follows: ***Reluctance*** within magnetic circuits that weakens flux at unaligned rotor and stator poles position. That is a clue that motor exciting electric power signals (i.e, phase commutation voltage pulses and current) carry rotor position information of varying reluctance due to deviating air spaces

between rotor and stator poles. The dynamic impedance model needs improvements that may include rotor position dependent parameter equivalent resistance and inductance components.

1.3   Contribution

The main contributions of this thesis towards sensorless rotor position estimation are given as follows:

1. A Per phase BLDC motor impedance model has been proposed by inspecting the frequency response of its off-line phase to phase impedance measurement. One of the most common motor phase models is a resistor in series with an inductor without considering the fact that inductance is a function of rotor position as it deviates with the change in air gaps between the rotor and stator poles during rotation. That is one of the main reasons, we highly recommend to replace ordinary motor phase model with the rotor position dependent model for BLDC motor. The frequency response of proposed motor model well matches the actual measured impedance points. Our motor phase dynamic impedance model, which is given by the Figure (4.5) in this thesis, represents as a resistor (R_1) and inductor (L_1) in series and another resistor (R_2) in parallel with an inductor (L_2). The proposed phase model parameters R_1, R_2, L_1 and L_2 have been estimated using the least mean square fit. The equivalent phase model parameters are quite consistent with least change in rotor position R_1 in series with inductor L_1 for maximum, medium and minimum inductances on rotor positions. Where an explicit change has been observed in parallel resistor R_2, series inductor L_1, and model parallel inductor L_2 vary with different rotor positions that make R_2, L_1 and L_2 rotor position dependent parameters.

2. Near standstill and low speed range sensorless rotor position estimation techniques, and the " **Extended EMF model**" have been applied on a Brushless DC motor with on-line dynamic parameter identification using phase energizing electrical signals, currents and voltages. The extended EMF model is preferred due to its on-line parameter

identification and rotor position estimation, which are equally effective for no load
to full load motor conditions. The motor switching controllers have their own inter-
nal high-frequency signal and motor parameters can be identified with the controller's
own internal high-frequency signal instead of utilizing expensive external signal injec-
tion methods. Later, motor stator estimated parameters, such as resistance and direct
and quadrature inductance values were compared with the off-line frequency based
impedance measurements of the stator using the LCR meter.

3. The extended EMF based brushless DC motor observer response has been improved
   using a pre-compensated linear quadratic regulator (LQR): explained in section(3.5) of
   this thesis. Considering the fact that the LQR based observers provide an optimal error
   reduction with respect to state feedback input ($u(t) = -Kx$) and input to the system ob-
   server reduces the performance index (J_c) to its minimum value; approximately equal
   to zero [4, 5]. A pre-compensated LQR based observer has been introduced to the ex-
   tended EMF model to ensure a fast and stable observer model. As the observer in the
   extended EMF approach replaces sensor position sensors. The accuracy of the estima-
   tion must be comparatively close to motor shaft speed sensors because the commutation
   process is dependent on rotor position information. Therefore, an observer efficiency
   matters greatly to ensure that the uninterrupted rotor position information supply can
   maintain a consistent speed for a set time.

4. The Internal Model Principle algorithm is used for determining a real-time representa-
   tion of the spectrum of the voltage and current signals. This method is preferred over
   FFT as it can track changes in the spectrum with tracking resolution of less than $\frac{1}{4}$
   period containing frequency harmonic extraction, and noise rejection. This model can
   be used to any range of frequencies. We applied the internal model principle on the
   brushless DC motor signals to find impedance model for this motor. We need to know
   the motor model to compare the coefficients and find the high frequency model, that is
   the reason we need to find per phase model with the frequency-based motor resistance

and inductance measurements via LCR meter first. This identified spectrum of the voltage and the current can be compared to the our new position dependent LR model to determine the position. This final step is beyond the scope of the thesis.

1.4 Thesis Organization

- **Chapter 2** presents an introduction to brushless motors such as switch reluctance motors and permanent- magnet synchronous motors, their principle of operation and their common features to determine a sensorless SRM shaft position estimation strategy that might be equally applicable to all types of brushless synchronous motors.

- **Chapter 3** provides the mathematical modelling of BLDC motors using electrical, magnetic, electromechanical properties, and parameters of mostly DC synchronous motors.

- **Chapter 4** is a brief summary of the data acquisition set-up, measurement , and fundamental understanding of the applied strategies. In data acquisition and measurement, the motor stator resistance and inductance were recoded for variable inductance rotor positions with LCR-meters. Whereas, motor stator voltages and currents were recorded with the help of computer based data acquisition using a NI-DAQ-card.This chapter also briefly describe the theory of the applied strategies and their implementation.

- **Chapter 5** presents the results, data analysis and data comparison of applied rotor position estimation technique, the 'Extended EMF model' with improvement in its observer on PMSM/BLDC motors. Moreover, a dynamic motor phase model has been proposed by inspecting the off-line motor phase impedance measurement with increasing frequencies.

- **Chapter 6** is a brief summary of the conclusion and future work of this research in progress.

Chapter 2

Literature Review

Numerous sensorless rotor position estimation and speed control strategies for brushless synchronous motors, such as SRM and BLDC, have been investigated briefly in this chapter. Brushless motors such as switched reluctance motors (SRMs) and interior and surface permanent-magnet synchronous motors (PMSMs) are the electronically commutated motors. As compare to PMSM, the SRM motors have double saliency due to salient poles on both stator and rotor. The permanent synchronous (PMS) motors are single salient due to permanent-magnet stakes on rotor and poles on the stator appear with direct proportion to the number rotor poles. The amount of the torque in PMSM depends upon the total number of magnetic poles of the motor. Contrary to this PMSM, and SRM are light weight, therefore, are highly recommended in high-speed/low-torque applications, and are capable of bearing high-temperature operating conditions. The inductance of the brushless DC motor under observation varies with rotor position and SRM is known for inductance based controllers. Therefore, it is essential to understand the geometry, principle of operation, similarities and differences, and applications of both brushless motors. Another purpose of this literature review is to explore the most suitable existing sensorless rotor position estimation in SRM, which can also be applied on BLDC motor, e.g. interior permanent- magnet synchronous machines (IPMSM) and surface permanent-magnet synchronous machine (SPMSM), too with the same degree of accuracy. Various rotor position estimation approaches such as Back-

6

EMF-based, inductance-based, state observer-based, artificial intelligence-based, Kalman fil-
ter based, parameter identification-based, and control theory-based have been investigated
for SRM and then a SRM control methods such as SRM commutation and vector control
are given. Similarly, inductance-based BLDC motor's rotor position detection strategies have
been discussed and a short BLDC motor's control review is given in which field oriented
control (FOC), Back-EMF zero-crossing detection (ZCD), direct torque control (DTC), and
parameter identification have been highlighted.

2.1   Principle of Operation

Variable speed motors can be classified into two categories, based on their principle of oper-
ation, such as electromagnetic and variable reluctance motors.

In the first type of motor, i.e., electromagnetic, the motor's shaft rotates by the interaction
of magnetic field of its stationary (stator) and rotating assembly (rotor). The motor torque
comes into play with a phenomenon accordingly, opposite poles on rotor and stator try to
align.

Contrary to first type, torque produces in second type (i.e., variable reluctance motors)
with variable reluctance of the active system due to intermediate uneven spaces between ro-
tor and stator solid state poles. Different material have different reluctance and varies with
material to material and their geometric characteristics e.g, air has the highest reluctance
of all and measured in Henry inverse. Air gaps (spaces) in ferromagnetic materials prevent
magnetic flux saturation in rotor and stator which enhances overall capacity to store more
magnetic energy. Therefore, torque for the second category follows the motion of the rotat-
ing assembly, rotor, tangentially from the higher region of reluctance towards the lower and
has more freedom to access robustness in speed variation than the first type. The switched
reluctance motor (SRM) falls under the second category of motors. Moreover, stepper and
brushless DC motors (BLDC) are also some of the widely used variable reluctance motors.
Electromagnetics is a widespread field of physics and based on four basic Maxwell's equa-

tions. Two of these equations are fundamental in understanding the basic motor and generator operations.

According to **Faraday's law of induction**, whenever a current carrying conductor with **n** number of turns is placed in a time varying magnetic flux, a potential difference induces at its ends in consequence. Whereas, **Lenz's law** determines the direction of the induced voltage, across the motor windings, in result of Faraday's law. Faraday's Law comes into effect if any of the given below conditions are fulfilled:

1. Enclosed flux density within a conductor contour is time variant.

2. The flux linking over the conductor spaces is time varying. For example, air gap variation within rotor and stator poles of the motors.

3. The projection of the magnetic field with respect to conductor surface area is time variant.

Voltage induces in a current carrying coil due to time change of flux linkage which is given by Equation (2.1). Equation (2.2) represents the linking flux(λ) relation with conductor inductance and current flowing through it. Since, Equation (2.3) can be obtained by substituting Equation (2.2) in Equation (2.1).

$$v = \frac{d\lambda}{dt} \tag{2.1}$$

$$\lambda = L_{(i,\theta_r)}i \tag{2.2}$$

$$v = \frac{d}{dt}L_{(i,\theta_r)}i = L_{(i,\theta_r)}\frac{di}{dt} + i\frac{dL_{(i,\theta_r)}}{dt} \tag{2.3}$$

The flux linkage of conductor and hysteresis are among the main causes of non-linearity in variable inductance motors. The SRM inductance based modelling is given in [6]. In macroscopic view, reluctance in magnetic circuits acts similar as resistance in electric circuits. The electric and magnetic fields interaction in Faraday's law point of view is given with Equation (2.4):

$$\mathcal{B} = \mu\mathcal{H} \tag{2.4}$$

where,

$$\mu = \mu_0\mu_r \tag{2.5}$$

$\mathcal{B}$ represents magnetic field density and $\mathcal{H}$ is the change in magnetic intensity relative to $\mathcal{B}$ and μ. Where, μ_0 is the magnetic permeability of free space constant which is $4\times10^{-7}\pi$ H·m^{-1} and μ_r is the relative magnetic permeability which is specific for each ferro-magnetic element. According to Heaviside (1892), "*Reluctance is ratio of magneto-motive force (MMF) amplitude to magnetic flux amplitude in electromagnetic circuits.*"

Hopskin's Law and **Ohm's Law** are given in Equations (2.6) and (2.7)

$$\mathcal{F} = \Phi\mathcal{R} \tag{2.6}$$

$$\mathcal{E} = \mathcal{I}R \tag{2.7}$$

$\mathcal{F}$ is the magneto-motive force (MMF), Φ is the magnetic flux , $\mathcal{E}$ is electromotive force, $\mathcal{I}$ is current, R is resistance, $\mathcal{R}$ is the magnetic reluctance which has SI-units ampere-turns per weber (or turns per Henry), $\mathcal{F}$: is magneto-motive force (MMF) which is measured in ampere-turns, and Φ (Phi) the magnetic flux: measured in webers.

Reluctance varies with different materials, deviating lengths and cross-sectional areas, for example, air and vacuum are of high reluctance materials and ferromagnetic materials e.g, soft iron etc, comprises low reluctance. The electromagnetic flux is inversely proportional to reluctance, therefore, magnetic flux weakens with increased amount of reluctance.

$$\mathcal{R} = \frac{l}{\mu_0\mu_r A_c} \tag{2.8}$$

$$\mathcal{R} = \frac{l}{\mu A_c} \tag{2.9}$$

2.2 The Desired Common Features of Brushless Motors

1. High-speed operation capacity.

2. Four-quadrant operation modes with high efficiency.

3. According to [7],"*Minimum number of controllable switches (preferably less than two) to reduce the cost of power electronic circuit as well as to minimize the cost of the attendant circuits such as gate drives and logic power supplies and also to minimize the volume of heat sinks.*"

4. Sensorless rotor position tracking.

5. A huge capacity to reduce the space of controller circuitry by using a minimum number of switches. Only two switches are necessary for the capability of executing torque to speed four quadrant region of operation.

2.3   Control Review of Switched Reluctance Motors

The switched reluctance motors are listed as the most suitable in emerging high speed applications in the automotive industry. The windings of the motor are on the stator only, which comparatively reduce the mass at the rotor and increase its robustness several times over the ordinary ac synchronous motors. The power density of SRM are slightly less than the PMSM and BLDC motors, and higher than the induction motors. The statement applies to low speed applications only, where on high speed applications, the SRM has equal power density to permanent-magnet synchronous motors. The SRM windings are electrically separate and have negligible mutual coupling. Electrical faults in one phase does affect the other phases due to the negligible mutual coupling. The SRM has its inherent rotor position transducer: the inductance. Inductance in SRM varies due to rotor position of the motor and alternating phase energizing current. The rotor position can be determined by measuring the inductance during inactive duration of each phase winding [8]. According to Lucas *et al.*(2000) non-linearities in SRM parameters such as hysteresis and electromagnetic flux interaction, complicate the rotor position tracking.

Among some common sensorless position estimation approaches, the Back-EMF based approaches are widely being applied in most of the commercially available SRM controllers. The Back-EMF is a voltage or electromotive force, that opposes the current which induces

it in the motor stator coils. Whereas, at motor start-up, the Back-EMF voltage becomes very feeble and corrupted with high Noise/Signal ratio at low speed which makes Back-EMF calculation meaningless at lower speeds. Therefore, SRM rotor position sensing for proper commutation using Back-EMF, is unreliable for standstill and high torque applications. Alternatively, phase exciting voltage and currents are present in the motor from the beginning. Therefore, rotor position can be predicted using voltage and current that can cover a wide range of SRM operating region, including stand-still, compare to Back-EMF approach.

Later this chapter, briefly explains common features of SRM and PMSM common features and their structural review, basic motor principle of operation, on-going SRM control schemes and applicable commutation techniques. Later, a short review on sensor based and sensorless rotor position estimation approaches will be highlighted. This chapter also provides the control review of BLDC motors that incorporates, its principle of operation and some of the most widely used current sensorless rotor position tracking techniques. The two main approaches such as Back-EMF based and another inductance based rotor position identification by injection of the high-frequency signal.

2.4   History

Switched reluctance motors date back to the beginning of 20th-century. During that course of time, numerous scientists and physicists around the world were experimenting with the newly discovered phenomenon of electromagnetics and its practical applications in control and automation. According to T.J.E Miller (2001), the evolution of SRM motor spreads over a span of more or less than thirty years. Most of the research documents found on SRM are the patents: at least 11 patents were published before the year (1976) and approximately a rough estimate number between 1,847 and 1,976 patents were published at the end of the year (1999). There is a list of researchers who claim the invention of SRM motors as their contribution, but no distinct person may earn the entire credit for this invention and design improvement.

2.5 SRM Structural Review

In construction, SRM stator always has stator winding and rotor does not contain any conductor or magnet other than the steel rotor laminated core. Besides their simple construction, SRM architecture has some pros and cons. For example, for pros, SRM is light weight due to steel laminated rotor which further makes it lower in cost and more efficient in high-speed requirements. In addition, SRM can be the most reliable motors due to their phases which are highly independent of each other physically, electrically and magnetically as compare to other motor types. Whereas in SRM's cons, these motors are noisier, SRM motors also
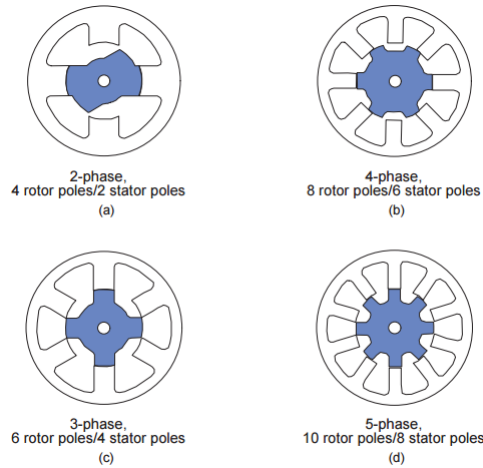
Figure 2.1: Various SRM geometries [9].

cannot directly operate on DC and AC excitation, they always need to be electronically commutated, and for that reason they need shaft position sensors (e.g., Hall effect sensors, flux gate current sensors, opto-coupler and resolver etc.,) to commutate at each instant with precision and accuracy. Last but not least, these motors are difficult to control as these are highly magnetically non linear and have more ripple in torque.

Figure (2.1) represents numerous SRM geometries with respect to phases, number of stator and rotor poles. At least two phases are required to start the motor and three to make sure the direction of motor rotation. More number of phases reduces the torque ripple in SRM. The SRM stator poles are not half the number of stator poles but they need to differ in

number to ensure motor rotation.

2.6   SRM Control

Direct correspondence of magnetic characteristics of synchronous motors (e.g., SRM and BLDC) to their rotor position is a clue to their sensorless control possibility.[10] *et at.* (2004) explained the possibility of rotor position estimation through identifying the the signature in active or an idle phase of the SRM. The same pattern detection of rotor position with respect to magnetic status of motor can be used to recover rotor position in SRM sensorless control. In the state-of-the-art, sensorless control techniques can be broadly classified into three categories:

1. Hardware intensive

2. Data intensive

3. Speed of instruction execution, millions of instruction in second, MIPs intensive
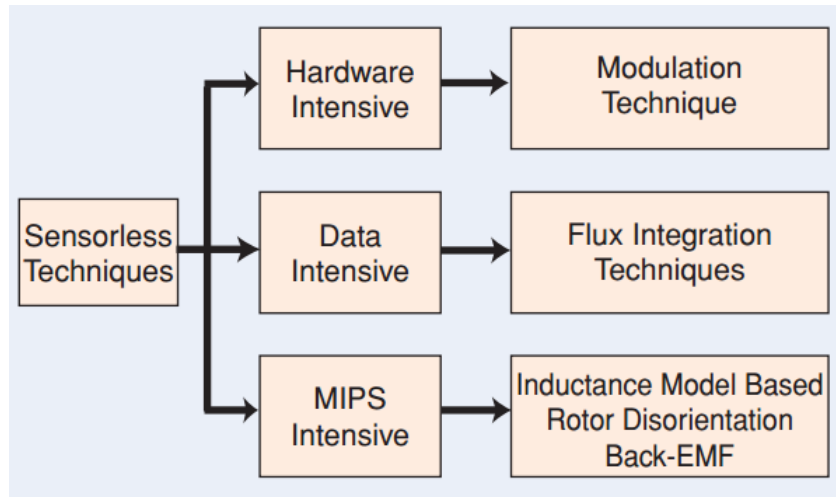
Figure 2.2: Ongoing SRM sensorless control techniques[10].

Figure (2.2) concludes the above mentioned control techniques as follows: **Hardware intensive control** magnetic information acquisition by using sensors which is not considered

suitable control technique. **Data Intensive control** magnetic signature of machines are or-
ganized in form of Look-up tables those calculate parameters of interest such as flux linkage
and inductance etc. Nevertheless, it is a simple, straight forward approach, overloads the
memory and processors while operation and sensitive to parameter variation. **MIPs inten-
sive** speed of Millions of instructions per second mainly depends upon the high speed signal
processors such as DSP-processors and FPGA (Field programmable gate array). SRM con-
trol with magnetic signature defining differential equations are put together to solve dynamic
behaviour of the system to obtain rotor position. Such speed control mechanism has high
sensitivity to parameter variations and gives lousy output on parameter variation.

Figure (2.3) interprets a typical SRM cascaded control. The main control routine block is
responsible for control signal generation to the semiconductor switches to execute current reg-
ulation and phase commutation. A comprehensive knowledge of reference current, commuta-
tion instants and sequence of excitations is integral for persistent motor speed control. Most
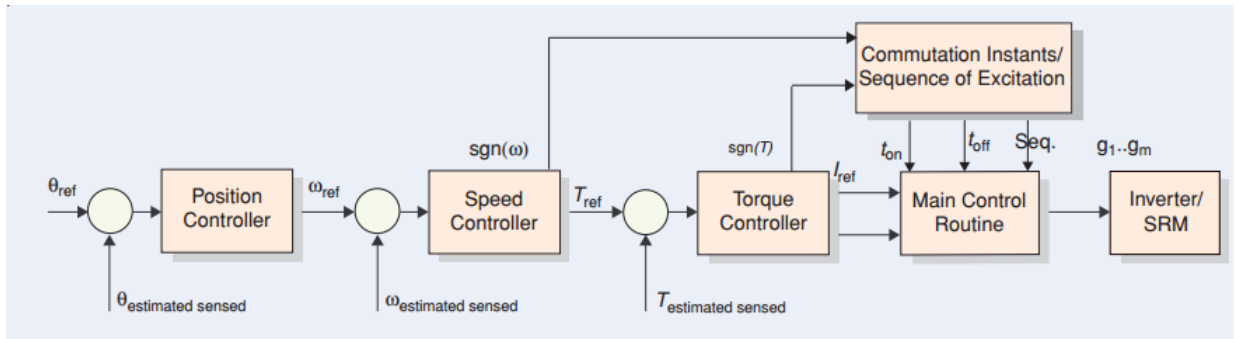
Figure 2.3: Typical cascaded control configuration for SRM [10].

importantly, **commutation** block requires rotor position through feedback sensors or esti-
mators, in order to conduct uninterrupted synchronous operation of motor. The common is-
sue with all SRM control approaches is that they provide fair resolution over limited speed
range. This is because SRM non-linearities make motor speed control quite challenging for
the entire speed control range.

2.6.1   SRM Commutation

According to Liu, X *et al.* (2011) two commutation approaches are the most effective which
are **Uni-polar phase excitation** and **Bi-polar phase excitation**, both can either be in si-
nusoidal or rectangular current wave forms. SRM motors mostly come with control switch
assemblies such as asymmetric full bridge, H-bridge and standard full bridge for variable
speed control with different stator pole configurations. Among them four quadrant variable
speed operation is well described for **4/6** SRM model where **4** is the number of rotor poles and
6 is number of stator poles in SRM model. Asymmetric full bridge and standard full bridge
inverters are preferred due to their simple switch configuration over H-bridge.

   Uni-polar phase excitation with asymmetric bridge is the most common SRM commuta-
tion scheme. Six electronic switches, turn on and off with proper sequence to excite phases to
meet consistent torque. (*See* Figure2.4) . Since uni-polar excitation exhibits low speed ranges
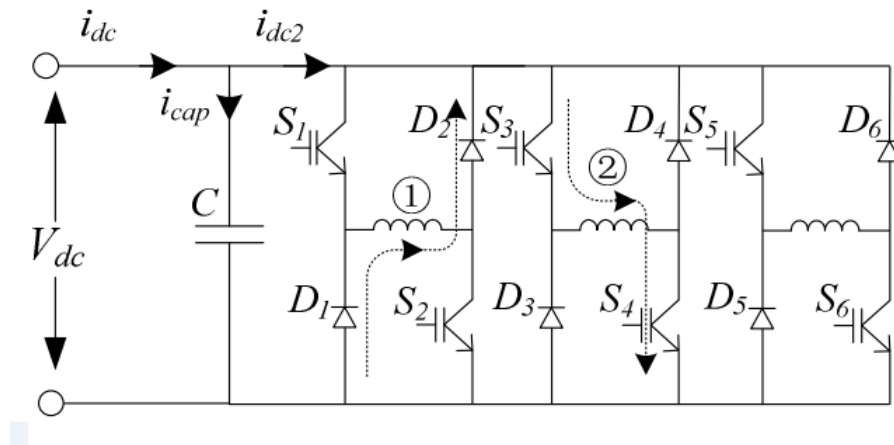
Figure 2.4: Asymmetric full bridge uni-polar phase excitation configuration [11].

with current pulse width modulation with rectangular waveforms. On the other hand, the same
scheme equally covers high speed range with voltage pulse width modulation.

   The rectangular **Bi-polar phase excitation** are recommended for low speed applications
but requires 60 mechanical degree turn-on as shown in Figures (2.6) and (2.7).   How-
ever, uni-polar rectangular excitation has the highest efficiency compare to sinusoidal uni-
polar excitation and bipolar rectangular excitation but causes more torque ripple and iron
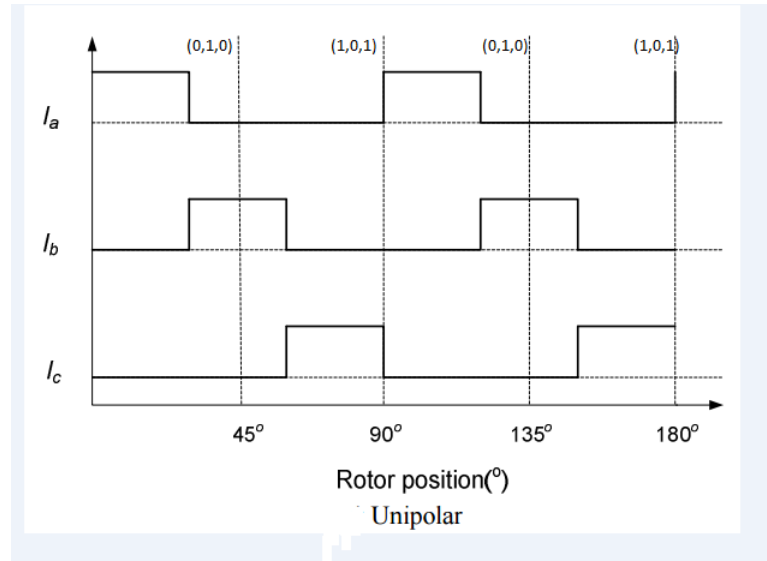
Figure 2.5: Commutation scheme for Uni-polar with current (PWM) rectangular wave excitation [11].
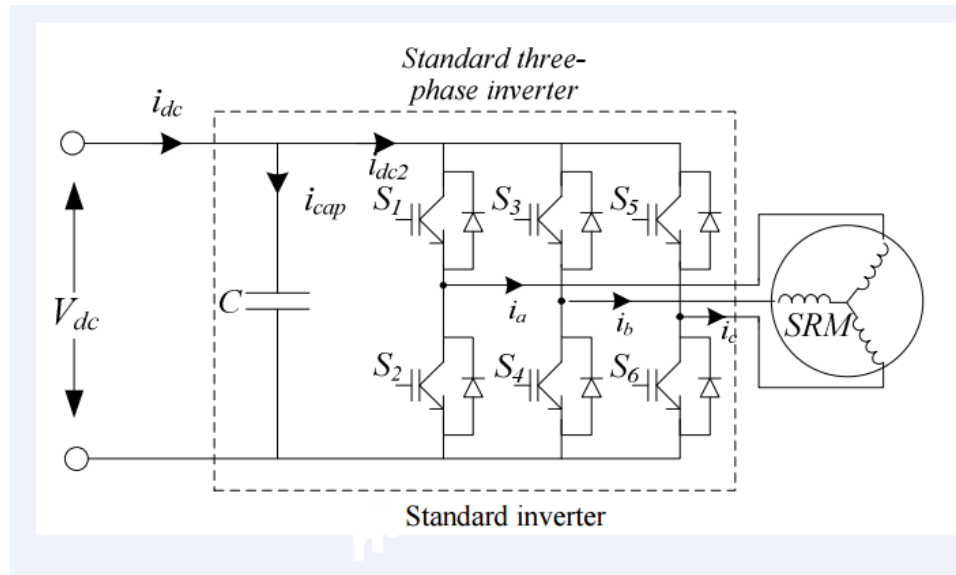
Figure 2.6: Bi-polar standard full bridge inverter [11].

losses.
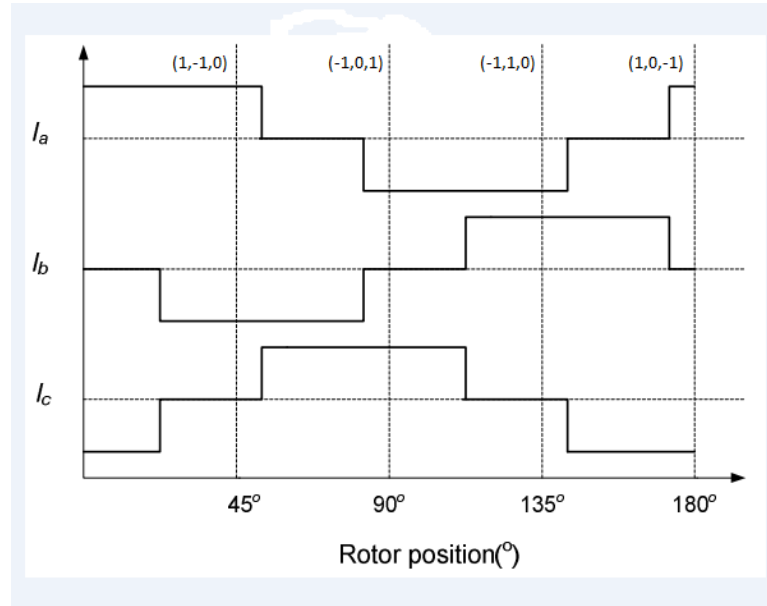
Figure 2.7: Commutaion scheme for Bi-polar with current (PWM)
rectangular wave excitation [11].

2.6.2   Vector Control

Nakao and Akatsu (2014) proposed a vector controlled-switched reluctance motor (SRM) drive
system. In this approach, a sinusoidal unipolar excitation current with DC offset is supplied
to each phase. An excitation current contains both the dc and ac component which creates
virtual flux in the rotor and rotating stator field. That's the reason, the SRM rotor saliency
diminishes and SRM behaves like single salient counterpart i.e, BLDC/PMSM motor. The
rotating stator field rotates at electrical velocity, interacts with rotor virtual flux and produces
electromagnetic force.

Vector control is well suited for on-line torque control, linear torque-current control and
maximum torque per ampere (MTPA) control. This technique simplifies the torque control
with least parameters requirement as shown in Figure(2.8).
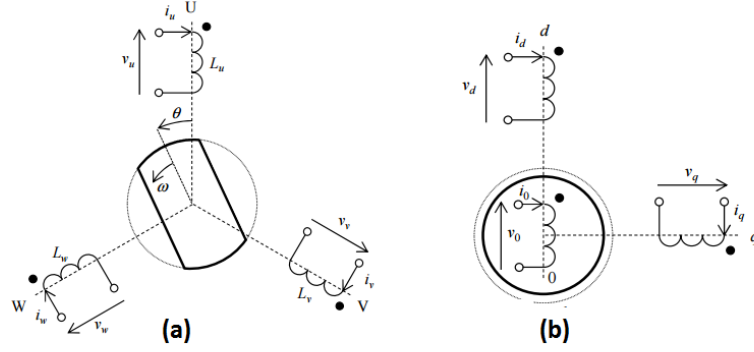
Figure 2.8: (a) Equivalent SRM 2 pole model on stationary frame. (b) Equivalent SRM model on rotating frame [12].

2.7   SRM Rotor Position Estimation

In order to control the SRM torque, phase current and absolute rotor position (sensor-based or sensorless) information is required for SRM proper electronic commutation. A brief comparative analysis of ongoing SRM rotor position tracking techniques with their pros and cons is given in this section. Later, inductance-based continuous, discrete and modern control approaches will be presented in respect of meeting the requirements of acquiring portability, cost effectiveness and instant rotor position estimation.

SRM control is dependent on *turn on angle* and *commutation angle* to maximize air gap torque. There are two ways to determine these angles, *absolute* and *incremental/variable reluctance* rotor position. In incremental method, a current reference requires a progressive information of *turn on angle* and *commutation* angle so, in this case, variable rotor position is measured. Whereas in absolute method, the control angles can be found with fixed reference rotor position for each stator phase (set of poles). Both the control angle approaches are available in continuous/discrete sensor based and sensorless control *chapter 8* of [8] .

2.7.1   Sensor Based Rotor Position Estimation

Resolvers are absolute position sensors which serve in multivariate industrial applications for position and speed of actuators. Resolvers operate like a rotary transformers with one rotating reference winding is energized with reference voltage (U_{ref}) and similarly the other two stator windings in Figure(2.9). The reference winding is fixed on the rotor and rotates with motor shaft's angular motion. The two stator windings are placed in quadrature apart from each other to generate the sine and cosine voltage signals such as, (U_{sin} and U_{cos}), respectively.
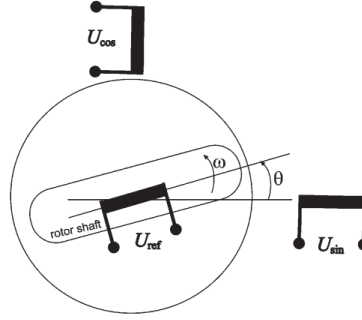
Figure 2.9: Schematic diagram of the basic operation of a resolver [13].

$$U_{sin} = A_1 sin(\theta) + B_1 + n_1 \qquad (2.10)$$

$$U_{cos} = A_2 cos(\theta + \phi) + B_2 + n_2$$

$$s_{\theta(t)} = U_{cos}(t) + jU_{sin}(t)$$

A_1 and A_2 are amplitude, B_1 and B_2 are off-set and n_1 and n_2 are the measurement of mean noise of signals *sine* and *cosine* of resolver signals. The frequency of U_{sin} and U_{cos} signals are identical to the reference voltage, and their amplitudes vary with respect to the sine and cosine of the shaft angle θ [13].

Variable reluctance (VR) sensors: such devices sense change in magnetic strength either by permanent-magnet or a coil wrapped around a ferromagnet cylinder energized with

DC source. The reluctance changes with change in the length of the air gap between the sensor and a ferromagnetic toothed shaft of the actuator. Additionally, frequency of the sensor output is the revolution per second of the shaft rotations. VR principle of operation is simple and comparatively inexpensive in its implications shown in Figure (2.10).

Another explanation of Faraday's Law of electro-magnetics brings forth an interesting relation between reluctance and rate of change of flux in electro-magnetic circuits. According to that, the variation in reluctance produces variation in the magnetic flux of the coil. Across the coil a voltage 'U' induces due to rate of flux $\frac{d\Phi(t)}{dt}$ which is bi-polar in nature [14]. The
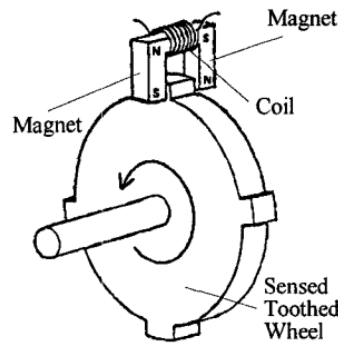
Figure 2.10: Variable reluctance sensor [14].

advantages of VR sensors are their simple construction, as it only needs a wire wrapped cylinder and, lower cost, ruggedness and reliability in intense temperature and chemical environment such as vehicle engines etc.

The disadvantage is the sensitivity to a number of sources of error: Vibrations or resonances sometimes induce voltage which reduces the **S/N** ratio of the device. This effect becomes worse at low speeds. Some extra pulses may be produced from the device leading to a loss of synchronism with respect to the sensed wheel. The measurement current in combination with the inductance of the coil leads to a phase shift at higher shaft speeds [14].

Hall effect sensors: were developed as an improvement in variable reluctance sensor explained in Figure(2.10). The magnetic circuit of Hall-effect sensors is comparable to the VR devices explained above, but instead of a sensing coil one or two (differential measurement

principle) the Hall elements are used to measure the changes in flux Figure (2.11): Due to the excitation current and the magnetic field, electrons within the Hall device experience a force (Lorentz force) resulting in a voltage at the edges of the Hall element.
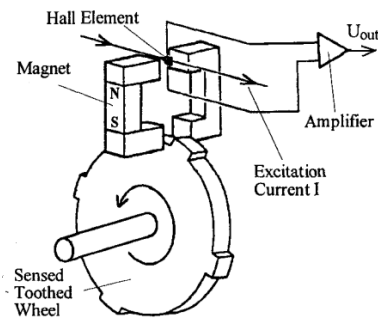
Figure 2.11: Hall effect sensor [14].
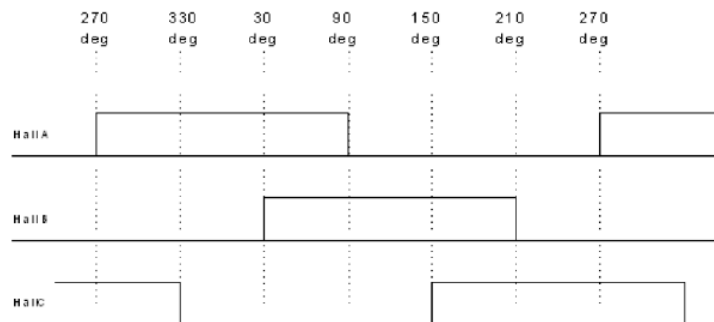
Figure 2.12: Three Phase Hall effect sensor output [3].

Hall effect voltage element bears direct relationship to the constant magnetic field for constant current. The operation of the Hall sensor is simple. The sensor electronics amplifies the Hall voltage, which generates a train of a square-wave output with respect to the frequency of the tooth wheel detection for a certain speed of rotor rotation. The disadvantage of hall effect sensor is its special installation on the stationary part of the motor and wire based sensing make this method rather more unreliable. One of the unattractive features of this sort of sensing is just 60° accuracy in rotor position measurement [14].

2.7.2   Sensorless Rotor Estimation Techniques

Continuous sensorless methods include invasive rotor position, as a function of the variable inductance based rotor position. In this method, an external known signal is injected into the system and then the processed signal is compared with the input reference signal with respect to inductance dependent parameters.

On the other hand, non-invasive rotor position identification incorporates continuous sensorless modern control, for example state observer and sliding mode control estimators. Rotor position estimators converge with respect to the SRM inductance slope. Practically, designed estimators do not converge with inductance slope in real time, the overload processors and occupy more space in memory during the process of computation. In this case, alternate artificial intelligence approaches e.g, neural network and fuzzy logic are computationally less intense and simple. These approaches need improvement in learning and adaptability. These approaches can be implemented in systems other than highly sophisticated servo-mechanism where performance discrepancies can be tolerated.

2.7.3   Back-EMF Based Control

In SRM sensorless control, continuous monitoring of Back-EMF is the most prominent approach in variable speed purposes. The motional voltage (Back-EMF) varies in direct relation with rotor speed in four quadrant operation such as standstill, torque, speed and position control. Figure(2.13) highlights the four regions between maximum torque to maximum speed where intermediary regions are of constant power region in which a wide range of speed can be achieved with proper commutation. Active parameters based on **Back-EMF** of the above mentioned regions in Figure (2.13) are given in Table (2.1) A speed controller may generate positive (i.e, motoring action) or negative (i.e, generator action) torque. Likewise, a position controller needs the information (clockwise) or (counter clockwise) speed.
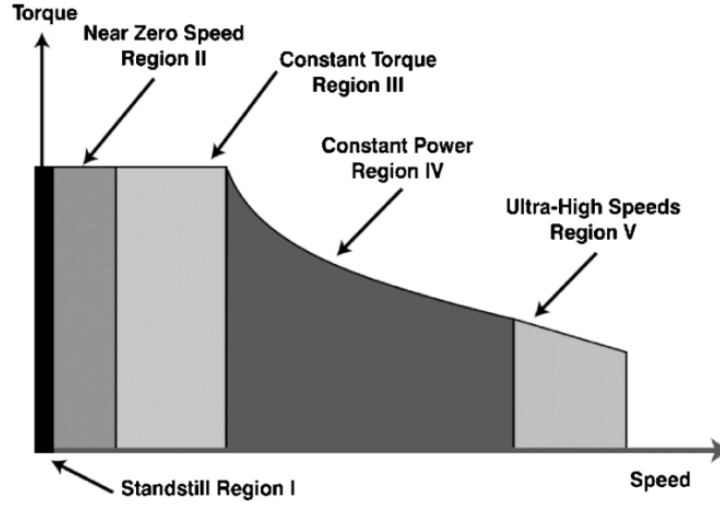
Figure 2.13: Four Quadrant variable speed regions of operation [15].

2.7.4 Standstill Control

Fahimi, B *et al.* (2004) describe standstill case in the cascaded variable technique based on Back-EMF voltage induces in motor action meeting any of the three conditions of the Faradays law as given in section (2.1). The reluctance of the magnetic circuit at standstill and near it does not vary. Therefore, the induced voltage in the coils of SRM is due to an increment of magnetizing flux in the stator core. The impedance of the motor phases can be found, using it's excitation signals, which consists of lumped parameters of the motor. These lumped

Table 2.1: SRM different regions of operation[15].

Region	Phase Voltage Equations
Region I	$V = Ri + \left(L + \frac{idL}{di}\right)\frac{di}{dt}$
Region II	$V = Ri + \left(L_{(i,\theta_r)} + \frac{idL}{di}\right)\frac{di}{dt}$
Region III	$V = \left(R + \omega\frac{dL}{d\theta_r}\right)i + \left(L_{(i,\theta_r)} + i\frac{dL}{di}\right)\frac{di}{dt}$
Region IV	$V = \left(R + \omega\frac{dL}{d\theta_r}\right)i + L_{(\theta_r)}\frac{di}{dt}$
Region V	$V = \omega\frac{dL}{d\theta_r}i + L_{(\theta_r)}\frac{di}{dt} + \Sigma M_m\frac{di_m}{dt}$
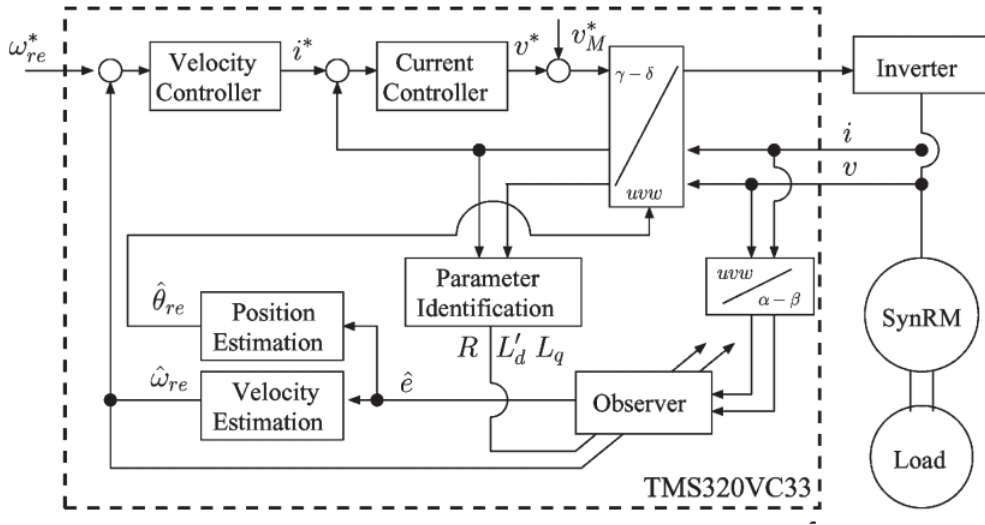
Figure 2.14: The extended EMF based motor sensorless control [16].

parameters are comprised of the resistances and inductances of motor phases and can well depict the dynamic behaviour of SRMs [10]. Note that self-inductance of the synchronous motors do not alter at standstill so in this case current non-linear saturation effect may be considered for better control in this region. Komatsuzaki *et al.* (2008) proposed a rotor position estimation at standstill, simply by computing the angle of state space vector of sinusoidal inductance. Rotor position is identified by supplying short duration DC voltage signal to idle phases during rotation. Again this approach is similar to short time signal injection approach.

Ichikawa *et al.* (2006) introduced an on-line parameter identification method and a sensorless control strategy to keep up position estimation accuracy, and sensorless control is acknowledged in both surface permanent-magnet synchronous motors (SPMSMs) and Interior permanent permanent-magnet synchronous motors (IPMSMs). This identification algorithm does not use motor position and velocity to identify motor parameters, whereas the identified parameters do not affect the accuracy of position estimation under the sensorless control.

2.7.5   Inductance Based Control

Jun Cai and Zhiquan Deng (2012) proposed SRM sensorless control technique, "*Phase current slope difference*", that determines each phase inductance for full-cycle with pulse injection technique. Where each phase inductance is considered as vector with fixed phase difference around that composed vectors rotate with rotor position. Furthermore, combining the composed vector orthogonal decomposition with inductance subregional method identifies the rotor position in Figure(2.15). A problem with external signal injection which sometimes is so feeble that identifying its presence in noisy environment becomes challenging and unreliable. Another inductance based SRM control technique for low speed applications, presented
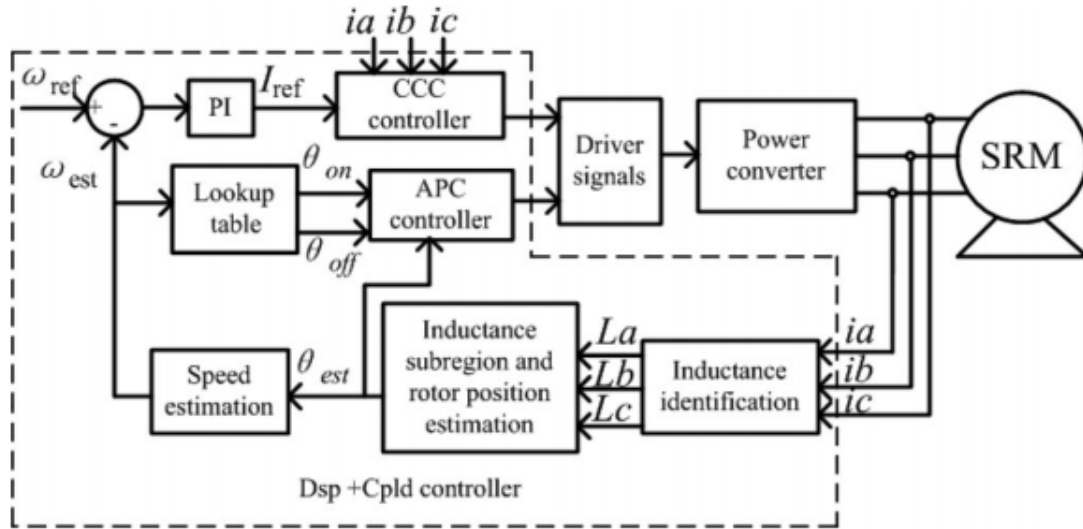
Figure 2.15: Inductance based SRM sensorless control [17].

by Hongwei *et al.* (2004), which estimates incremental inductance using terminal phase for the entire rotor rotation. This approach compares incremental inductance model to an analytical model. Such comparison constructs a relationship between incremental inductance, phase current, rotor position to estimate the rotor position.

In an ideal SRM current gradient control, constant current is supplied for the positive inductance slope ($\frac{dL(\theta)}{d\theta}$) in case of its motor action and to the negative inductance slope in

generator action [18, 19, 20].

$$T = \frac{1}{2}i^2\frac{dL(\theta)}{d\theta} \tag{2.11}$$

As SRM inductance varies with each rotor angular displacement increment. Based on inductance knowledge, three angles on the rotor are marked as follows:

1. θ_{on} (turn on angle usually unaligned position).

2. θ_{off} (i.e., turn off angle, an angle a little prior to aligned position).

3. θ_{con} is conduction or excitation angle which is difference of turn on angle and turn off angle $\theta_{con} = \theta_{on} - \theta_{off}$.

Figure (2.16) Conduction angle or excitation angle is sometimes known as dwell-angle as well [18]. In order to acquire maximum torque, θ_{on} should be carefully chosen as for at braking torque (i.e., negative gradient) θ_{on} must remain active.

For chopping (PWM) operation of phase current on the completion of turn off angle negative voltage is applied to reduce the current. One problem with method of rotor position estimation is that current signals are not available at starting. Therefore initiating procedure needs a separate set up. Such a step is very similar to BLDC sensorless drive. For acquiring sufficient current gradient signal, by building enough open loop SRM start up speed with programmed frequency vs time feature [19].

2.7.6   State Observer Approach and Artificial Intelligence Methods

Li Yu-zhou *et al.* (2010) considered the non-linearities in magnetic flux coupling and cogging torque and estimated the switched reluctance model based on state observer approach using *Enhanced Kalman Filtering (EKF)*. This approach linearises the switched reluctance model recursively and also keeps a precise track of variable speed. The problem with this method is, that state observer rotor position estimation do not converge with actual system in real time.
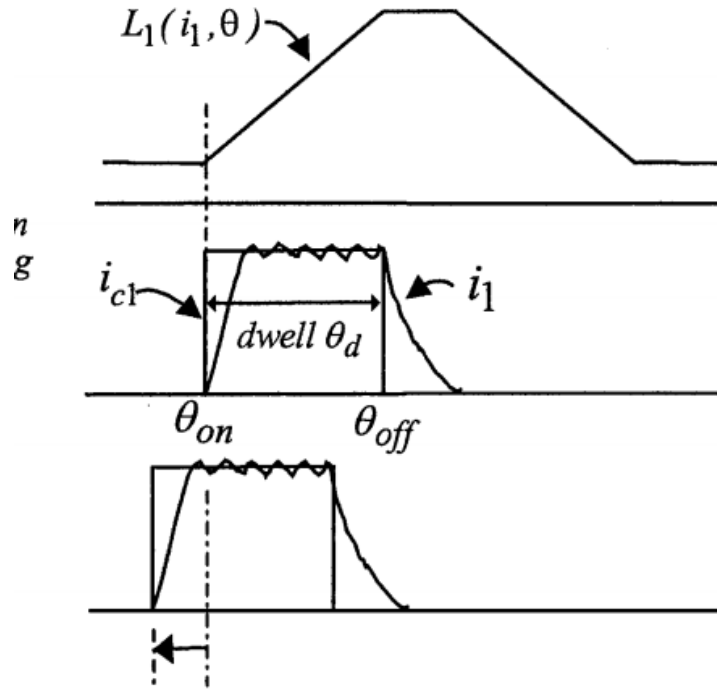
Figure 2.16: Conceptual SRM Inductance variation in commutation tuning control [20].

As mentioned in section (2.7.2) above, that state observer based rotor position estimation techniques devoid of computation simplicity and requirement of less memory. Paramasivam *et al.* (2003) elaborate SRM rotor position estimation based on *Adaptive Network based Fuzzy Inference System (ANFIS)*. Where ANFIS uses first order Sugeno-style fuzzy system with flux Ψ and current i as inputs to give rotor position θ as output of the multi-layer fuzzy logic system. This approach determines standstill rotor position by injecting short duration voltage for approximately 2 s. The modern control theory based on the following approaches, such as state-observer and artificial intelligence approaches, suffer from differences between estimated system to real system convergence and adaptability issues.

2.8   Torque/Speed Regions of Operations

According to [21],"*High torque for starting, at low speeds and hill climbing and high power*

for high-speed cruising. Wide speed range, with a constant power operating range of around

3 to 4 times the base speed being a good compromise between the peak torque requirement of

the machine and the volt-ampere rating of the inverter." Figure (2.17) is an ideal torque/power-

speed characteristic curve, divided into three regions and signifies the speed in machine trac-

tion applications:
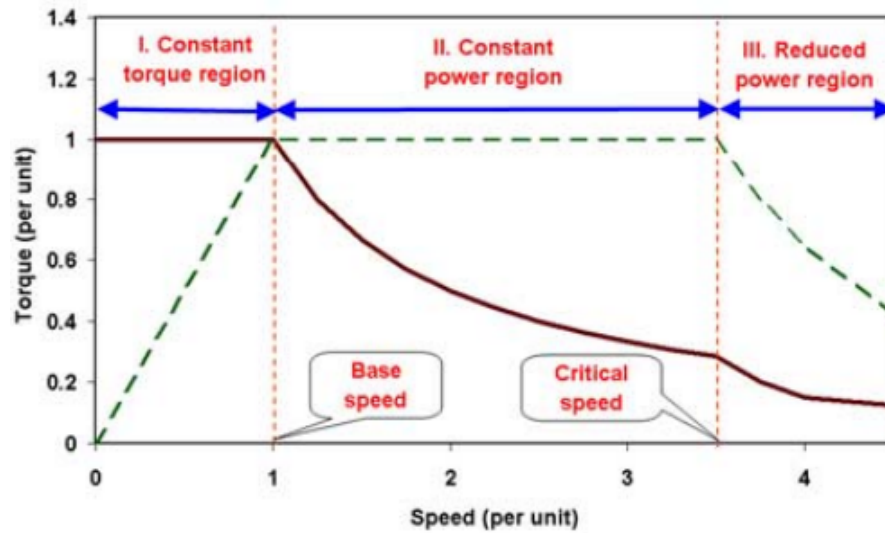
Figure 2.17: Idealized torque/power-speed characteristics[21].

1. constant torque I-region.

2. constant power II-region.

3. reduced power III-region.

In Figure(2.17), the **region-I** is a region of maximum constant torque which is due to current

controller constant current, **region-II** is region of constant power commutation which be-

comes effective due to subsequent phase limiting in voltage and current. **Region-III**, reduces

in power due to dominating **Back-EMF**, where motor speed is maximum and lowest is the torque .

The switched reluctance motors are suitable mechanical power actuators in various applications. Different electrical automotive companies all over the world have developed control drives for a variety of power range as low as (3 hp), medium power (300 kW) and high power upto (1000 hp). Similarly, control drives are also in massive development for speed ranges from 4500 rpm to at least 50,000 rpm serving different speed purposes [8].

2.9 Brushless DC Sensorless Control Review

Ikhlas presented a brief summary of brushless DC motors and their control review as follows: Three phase BLDC motors are driven by pulse modulated voltage signal to each phase known as electronic commutation. Three modulated voltages, $\frac{1}{3}$ of cycle degree apart from each other in three phase, energize active phases at particular angles. The criterion of these angles is based on the stator, synchronously rotating, and rotor flux orientation and linking. In order to get the maximum torque, BLDC stator and rotor fluxes must be at 90° apart to each other. Most of the common BLDC control approaches are:

1. Field orientation control (FOC) which is also called Vector control.

2. on to torque generation **Back-EMF** zero-crossing detection.

3. Direct torque control (DTC).

4. Parameter Identification.

5. Special inverter pulse width modulation (PWM) patterns.

In order to detect those angles, sensors track rotor position continuously, and based on the signal, the rotor position is detected respectively. Motors are supplied with free-wheeling bridge inverters which automatically apply voltage pulses to the desired phases for continuous motor operation.
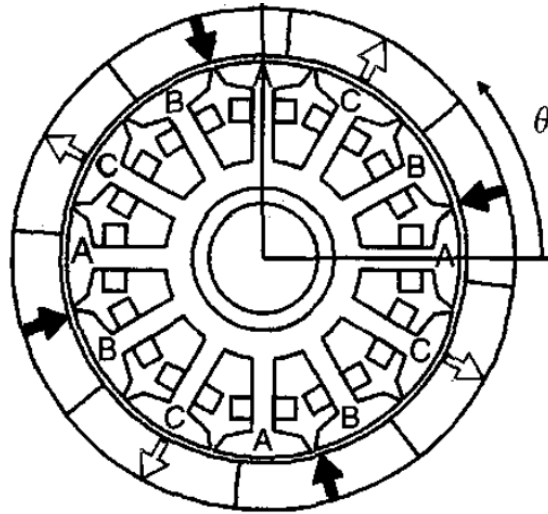
Figure 2.18: 8 pole and 12 slot Brushless DC motor [22].

2.9.1 Principle of Operation

Ikhlas gives a detail review of BLDC motors as follows, the brushless DC motors are uni-salient synchronous motors and require continuous tracking of rotor position from rest mode to fully operating state, for proper electronic commutation. As brushless DC motors do not embody solid state brushes for commutation which are more robust and efficient in performance. A proper supply of voltage strokes depends upon rotor position estimation precision to signal right electronic switches in inverter bridge to energize subsequent phase coil to keep up steady motor operation. Figure (2.19) illustrates the least control requirement blocks for
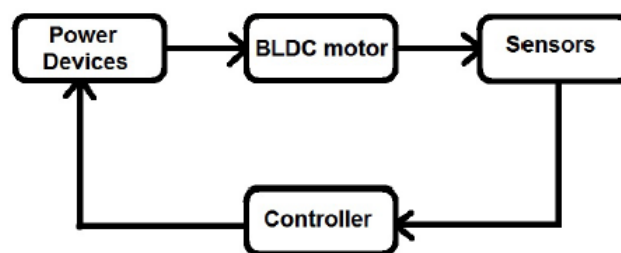
Figure 2.19: Brushless DC operation [3].

BLDC motors. Power devices supply power to BLDC motors which convert the electric energy into mechanical energy in the form rotation of the motor shaft. Rotor position sensing devices, sensors/transducers convert mechanical energy into electrical signals to update the controllers for speed controlling purposes.

2.9.2   Inductance Based Rotor Position Estimation

Ikhlas highlighted two inductance based sensorless BLDC control techniques. The **first**, is a pulse-based algorithm, which determines rotor position by monitoring the relative stator to rotor variable inductance. This method of rotor position detection, is exhibited with variable response times as the current changes with various rotor positions. The **second** technique is similar to one of the switched reluctance motor inductance speed control based techniques as explained in section (2.7.5). In this method, a current pulse is injected into all six segments of any electrical cycle and then is put to an inductance variation impact over current rise time and fall time.

2.9.3   Pulse Width Modulation Based Approach

Boussak (2002) used an alternate sensorless initial rotor position estimation approach using a *Kalman filter* based parameter estimation for BLDC motor for low speed. Initial position estimation is challenging if the motor is already in a continuous motion. Most applied sensorless rotor position estimation techniques involve **Recursive least square** or **Kalman filter**, to extract rotor position from voltage and stator current information by the process of estimation. Initially, on the start-up phase voltage and stator current are both zero, therefore, initial position cannot be found this way. This approach has been applied on the IPMSM which is more complex due to its asymmetric magnetic circuit. Therefore, initial position can be predicted by inspecting the current response of the applied voltage at a standstill. Nevertheless, the only useful rotor information can be determined using phase inductance which is a function of rotor position of PMSMs.
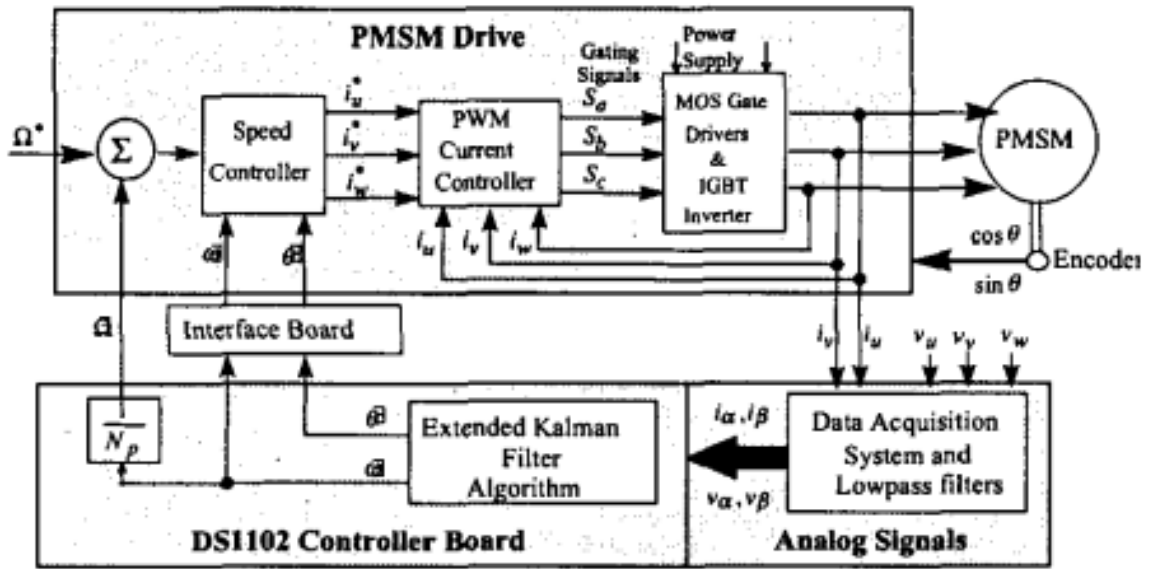
Figure 2.20: Extended Kalman filter based sensorless speed control strategy[23].

The given approach proposes the fundamental components of applied pulse width voltage strokes and resulting current at a standstill.

2.10   Summary

This chapter constructs a brief understanding of synchronous motors whose inductance is a function of their rotor position e.g, SRM and PMSM/BLDC motors. Further, basic physic laws, which define these motors' principle of operation and some of their common features, have been highlighted in detail for both types of the motors. SRM is a very good example of salient pole motors that help in understanding the rotor position estimation in single salient synchronous motors more explicitly and also draws a simple rotor position estimation understanding for double salient motors as well. The electronically controlled brushless motors are driven with synchronous speed with persistent supply of voltage to motor phases in particular sequence using different commutation strategies (i.e, six step, sinusoidal or trapezoidal commutation) with respect to rotor position. Usually, rotor position sensors are used for this purpose. Recently, sensorless techniques such Back-EMF based, pulse width modula-

tion based and motor parameter on-line estimation based with high frequency signal injection techniques are replacing sensors. The next chapter explains the sensorless rotor position estimation motor modelling.

Chapter 3

BLDC Motor Modelling

Separately excited dc motors and synchronous motors have two sources of excitations, one for the field and other for the phase coils, the armatures. Whereas torque in these motors is proportional to the product of the armature and field coil current. For linear operation, field magnetizing current is kept constant while varying the winding coil current to provide air gap torque. Non-linearities in most of the AC and DC motors are due to three phenomena:

• The B-H characteristics of the magnetic model of the AC/DC synchronous motors.

• The phase flux linkage is dependent upon the phase current and rotor position.

• Single source of excitation [8].

This chapter gives an introduction to brushless DC motors modelling. Motors convert electrical energy to produce mechanical output by interacting electric and magnetic fields. A general BLDC model has been given in [3] and inductance was found to be not constant.

Ichikawa *et al.* (2006) gives mathematical model which is applicable to all types of AC and DC synchronous motors. Further an introduction to EEMF model will be presented for stationary and on rotating frame. EEMF model is based on motor parameter identification which is capable of sensing rotor position with magnetic saturation or rotor saliency at a wide range of speed including standstill and low speeds. A general view of BLDC motors magnetic

properties, electrical properties will be given in this chapter then EEMF based model will be explained.

3.1 Magnetic Model

Magnetic field in BLDC motors are produced due to two main sources of magnetic flux. First, the permanent-magnet flux ϕ_{mag} due to magnetic characteristics of permanent-magnet materials on rotor with fixed magnetic density. Whereas the second flux type ϕ_{coil} is due to the stator winding current which sets up synchronous rotating magnetic field which rotates with the motor power supply frequency. The rotating electromagnetic field is produced in the motor stator with the increasing and decreasing flow of current magnitude in three windings (i.e., motor phases) with certain sequence. The current increase in the first energized winding produces a magnetic field aligned with this stator pole. Then current in the second winding starts increasing, at this point the magnetic field begins to rotate towards the second stator pole. The current is then reduced in the first phase allowing the magnetic field to further rotate until then the first current is zero and the field is perfectly aligned with the second stator pole. At last the current rise begins in the third winding which further shifts the magnetic field. The relationship between electrical frequency and mechanical speed of the synchronous motors is given by Equation(3.1):

$$N_s = 120\frac{f}{P} \tag{3.1}$$

N_s is the *"Synchronous Speed"*, f is *"Power supply frequency (Hz)"* and **P** is *"Number of pole pairs"*.

Continuous rotating magnetic field comes into play due to uniformly distributed windings within BLDC stator slots which are in synchronization with rotor magnet pole pair. The total flux is the combination of magnetic flux of stator and permanent magnetic flux of the rotor as given in Equation(3.2):

$$\phi_{tot} = \phi_{coil} + \phi_{mag} \tag{3.2}$$

Therefore, the total magnetic flux of BLDC motors divides into two magnetic flux quan-

(a) Demagnetization effect   (b) Enhanced magnetic effect
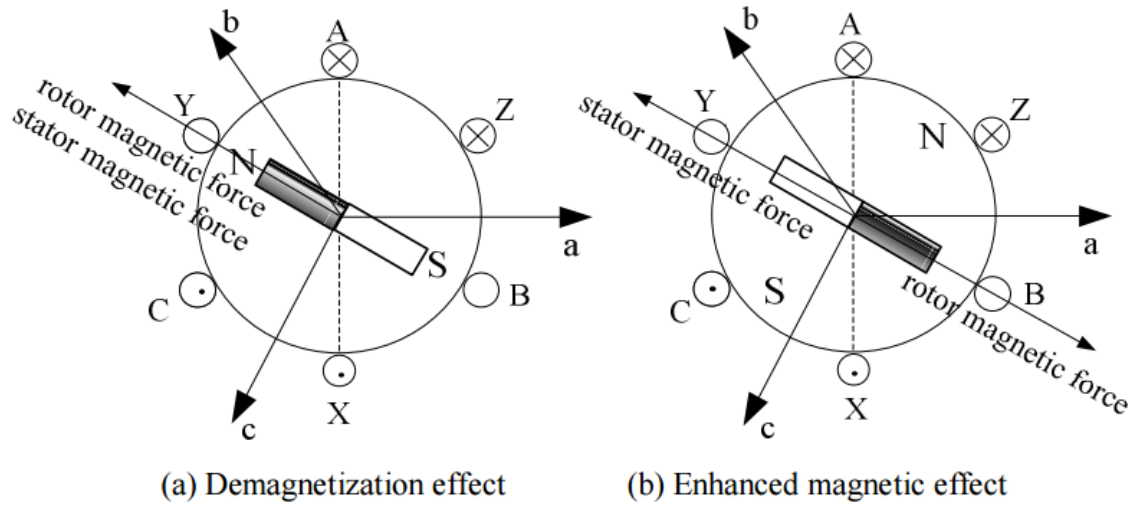
Figure 3.1: BLDC motor's magnetic model[24].

tities and is represented separately in magnetic model [25, 3]. Equation (2.4) explains the permanent- magnet mathematical expression which further portrays the magnetic field strength according to varying materials and impacting geometries.

3.2   Electrical Model

Electric characteristics of BLDC motors depends upon excitation current, voltages, flux linkage, and number of turns/coils per unit phase winding conductor. The Figure (3.2) gives an equivalent circuit for BLDC motor in which the rotor is modelled by rotor resistance in parallel with constant current source, since direction of current source points toward North pole and provides rotor fixed flux ϕ_r and ϕ_T is total flux due to stator and rotor. Similarly, stator is given by constant voltage source with stator resistance in series and overall flux linking in the electromagnetic circuit. Notice that the given model above ignores the time varying inductance and requires improvement.

Flux linking is mainly due to current in winding and rotor permanent-magnet. Using figure
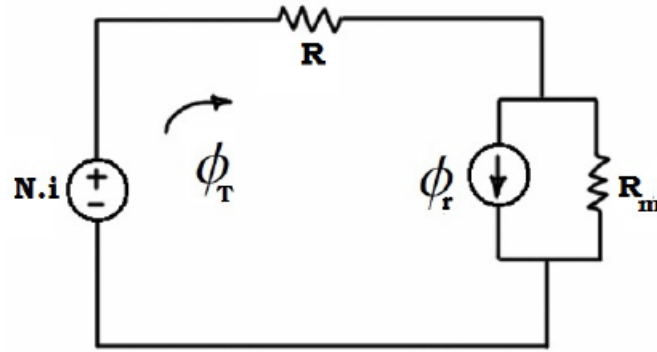
Figure 3.2: Equivalent simplified BLDC motor schematic diagram [3].

(3.2) flux linking expression can be given by Equations (3.3 and 3.4),

$$\lambda_s = N \times \phi_T = \frac{N^2 i}{R + R_m} + N\phi_m \tag{3.3}$$

$$L = \frac{N^2}{R + R_m} \tag{3.4}$$

where Equation (3.4) depicts the equivalent winding inductance and so substituting this equation in Equation (3.3). The BLDC equivalent electrical model can be represented by the Figure (3.2) in terms of simplified inductance model.

$$\lambda_s = Li + N\phi_m \tag{3.5}$$

The phase inductance is a function of both time varying current and rotor position therefore, Equation (3.6) becomes as follows:

$$\lambda_s = L(\theta_r, i)i + N\phi_m \tag{3.6}$$

[3].

3.2.1 Electromagnetic Model

Most of the BLDC motor per phase models, ignore rotor position dependent inductance. BLDC electrical model can simply be presented by the following Equations (3.7 and 3.8) assuming

that phase coupling is negligible.

$$V = Ri + \frac{d\lambda_s}{dt} \tag{3.7}$$

Equation (3.7) can also be written as follows:

$$V = Ri + L(\theta_r, i)\frac{di}{dt} + i\frac{dL(\theta_r, i)}{d\theta_r}\frac{d\theta_r}{dt} + \frac{Nd\phi_m(t)}{dt} \tag{3.8}$$

First term of the Equation (3.8) is due to the voltage dissipation in windings to overcome resistive losses of the motor, the second term represents the change of magnetic energy stored as a result of changing current and the last term is an alternate of Back-EMF. It is important to note that inductance is the function of rotor mechanical angle and amount of the current passes through it. Therefore a precise rotor position can be extracted through motor inductance on a wide range of speed. Unfortunately in Back-EMF constant (K_b) calculation, inductance is not considered as function of rotor position which causes the Back-EMF based rotor position schemes to be unable to detect initial rotor position at start.

$$\mathcal{E} = i\frac{dL_{(\theta_r, i)}}{d\theta_r}\omega_r = K_b\omega_r \tag{3.9}$$

However for simplification, the per phase model ignores the rotor position dependent terms.

$$\frac{dL_{(\theta_r, i)}}{d\theta_r} = \frac{L_{(aligned)} - L_{(unaligned)}}{\theta_{r(aligned)} - \theta_{r(unaligned)}} \tag{3.10}$$

Equation 3.10 represents the stator rotor poles aligned and unaligned flux linking in rotation. Since this inductance slope is constant between symmetrically distributed rotor pole position and clearly helps finding out mechanical rotor position to provide initiating commutation signal at start up. A suggested BLDC per phase model has been given with variable inductance calculated for each 2mm radian increment for the entire rotation in AB phase in chapter 4.

3.3   Inductance Invariant Model

A state space model, is given by Equation (3.11)

$$
\begin{bmatrix} \dot{i} \\ \dot{\omega}_r \\ \dot{\theta}_r \end{bmatrix} = \begin{bmatrix} -\frac{R}{L} & \frac{-K_e}{L} & 0 \\ \frac{K_t}{J_m} & \frac{-K_f}{J_m} & 0 \\ 0 & 1 & 0 \end{bmatrix} \times \begin{bmatrix} i \\ \omega_r \\ \theta_r \end{bmatrix} + \begin{bmatrix} \frac{1}{L} & 0 \\ 0 & \frac{-1}{J_m} \\ 0 & 0 \end{bmatrix} \times \begin{bmatrix} V \\ T_L \end{bmatrix}
\tag{3.11}
$$

$$
\begin{bmatrix} i \\ \omega_r \\ \theta_r \\ T_e \end{bmatrix} = \begin{bmatrix} 1 & 0 & 0 \\ 0 & 1 & 0 \\ 0 & 0 & 1 \\ K_t & 0 & 0 \end{bmatrix} \times \begin{bmatrix} i \\ \omega_r \\ \theta_r \end{bmatrix}
$$

for BLDC motor had been derived in [3] using basic electric, magnetic and mechanical model of the motors. The model is based on the fundamental physics laws which define the mathematical characteristics and relations of the intermediary systems equations. This mathematical modelling of BLDC motors lacks in information to define magnetic saturation, reluctance and resulting inductance change based on the these parameters. This model considers that inductance of the system is invariant through the steady state operation.

3.4   Variable Inductance Model

• **PMSM Model at rotating reference frame** : Equation (3.12), taken from [16], is a general mathematical representation for all synchronous motor types. The motor driving signals such as voltage, current and inductances are represented in form of *'Direct and Quadrature axes'* in synchronous motor models.

$$
\begin{bmatrix} V_d \\ V_q \end{bmatrix} = \begin{bmatrix} R + \rho L_d & -\omega_{re} L_q \\ \omega_{re} L_d & R + \rho L_q \end{bmatrix} \times \begin{bmatrix} i_d \\ i_q \end{bmatrix} + \omega_{re} K_e \begin{bmatrix} 0 \\ 1 \end{bmatrix}
\tag{3.12}
$$

In order to understand the above given per phase synchronous motor model we need to understand the physical meaning of the 'Park's transform' in rotating and stationary frame references.

Reluctance is a property of a magnetic circuit that opposes the magnetic flux lines, which is the ratio of magneto-motive force to magnetic flux [26]. The inductance of the motor windings is inversely proportional to their corresponding reluctance as follows:

$$L = \frac{\lambda}{i} = \frac{N^2}{\mathcal{R}}$$

(3.13)

Where in the Equation (3.13) λ is the flux linking, $\mathcal{R}$ is reluctance, L is the stator inductance, and i is stator current.
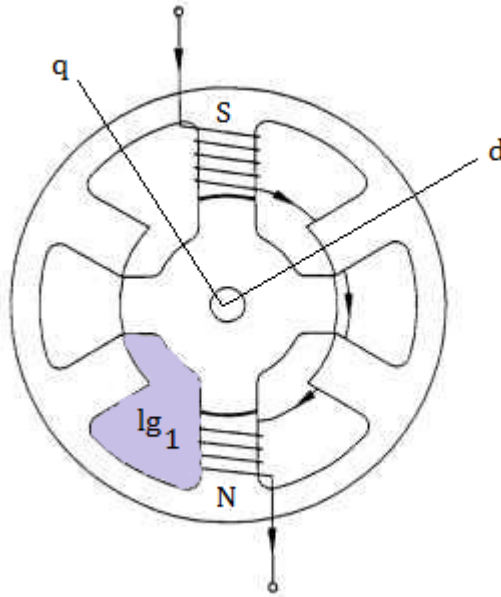
Figure 3.3: Direct axis and quadrature axis inductance and reluctance relationship.

A good explanation of direct and quadrature axis reluctance by means of mechanical construction of permanent-magnet synchronous motors has been vividly explained [27]. However, for simplification we have assigned variables l_{g1} and l_{g2} for unaligned and aligned poles air gap lengths.

$$\frac{\mathcal{R}_d}{\mathcal{R}_q} = \frac{l_{g2} + l_m}{l_{g1}}$$

(3.14)

Where

- $\mathcal{R}_d$ is the reluctance of the direct axis flux path.

- $\mathcal{R}_q$ is reluctance of the quadrature axis path or (90^0) of the flux path.

- l_{g1} is the air gap of the yoke. Note when poles are unaligned.

- l_{g2} is the air gap between the toothed poles. Note when poles are aligned.

- l_m is the thickness of the magnet.

The Figure (3.3) is representing the relationship between direct and quadrature inductance and reluctance of salient pole motors with respect to Equation(3.14). The reluctance of the direct axis $\mathcal{R}_d$ is relatively less compare to the quadrature axis reluctance, because of $l_{g2} \ll l_{g1}$. Therefore, inductance on the direct axis is maximum and minimum at quadrature axis. Where voltage and current on rotating reference axis transform from three phase AC signals to a simple two DC signals along the direct axis and quadrature axis respectively.

- **PMSM Model at stationary reference frame**: The Equation (3.15), which is taken from [16], is the synchronous motor model on stationary axis. In this model the second term contains the rotor position information as rotor position θ_{re} is a function of motor Back-EMF K_e, generated by permanent-magnets in result of rotation. Whereas, another term $Q(2\theta(re))$ is the rotor saliency.

$$\begin{bmatrix} V_\alpha \\ V_\beta \end{bmatrix} = \{RI + \rho\left(L_o I + L_1 Q(2\theta_{re})\right)\} \times \begin{bmatrix} i_\alpha \\ i_\beta \end{bmatrix} + \omega_{re} K_e \begin{bmatrix} -sin\left(\theta_{re}\right) \\ cos\left(\theta_{re}\right) \end{bmatrix} \tag{3.15}$$

Where,

$$L_o = \frac{L_d + L_q}{2} \tag{3.16}$$

$$L_1 = \frac{L_d - L_q}{2}$$

the L_o and L_1 are the average inductance values on direct and quadrature axis [16].

3.4.1 Extended EMF model

PMSM EEMF model at rotating frame: The Equation (3.17), which is taken from [16], is a mathematical model for synchronous motors on a rotating frame axis. Whereas Equation (3.18) is an equivalent model for the synchronous motors but on the stationary frame. This equation is a symmetrical form of Equation (3.12).The second term in this equation is called the extended EMF.

$$\begin{bmatrix} V_d \\ V_q \end{bmatrix} = \begin{bmatrix} R + \rho L_d & -\omega_{re} L_q \\ \omega_{re} L_q & R + \rho L_d \end{bmatrix} \begin{bmatrix} i_d \\ i_q \end{bmatrix} + \{ (L_d - L_q)(\omega_{re} i_d - \dot{i}_q) + \omega_{re} K_e \} \begin{bmatrix} 0 \\ 1 \end{bmatrix} \tag{3.17}$$

PMSM EEMF model at stationary frame:

$$\begin{bmatrix} V_\alpha \\ V_\beta \end{bmatrix} = (R + \rho L_d) I \begin{bmatrix} i_\alpha \\ i_\beta \end{bmatrix} - \omega_{re}(L_d - L_q) J \begin{bmatrix} i_\alpha \\ i_\beta \end{bmatrix} + \begin{bmatrix} e_\alpha \\ e_\beta \end{bmatrix} \tag{3.18}$$

$$\begin{bmatrix} e_\alpha \\ e_\beta \end{bmatrix} = \{ (L_d - L_q)(\omega_{re} i_d - \dot{i}_q) + \omega_{re} K_e \} \begin{bmatrix} -sin(\theta_{re}) \\ cos(\theta_{re}) \end{bmatrix} \tag{3.19}$$

The Equation (3.19) is the only derivative of the current component in Equation (3.18). The extended EMF is due to electromotive forces created due to permanent-magnet as well as rotor saliency. For every distinct rotor position of a PMSM, the Extended EMF has a unique ordered pair (e_α, e_β) value.

3.4.2 Parameter Identification with the extended EMF Model

For a reasonable parameter estimation of lumped parameters of motor model, the initial values of the motor velocity and position are required. The recursive estimation of parameters then keep updating the dynamics of the system. In order to make the parameter estimation matrix (Θ) in the RLS algorithm independent of motor velocity and rotor position, the **Characteristics of parameter matrix** is used and accuracy of the parameter estimation remains unaffected. The model state variables (x_{11}, x_{12}, x_{21}, and x_{22}) need to be added such that the system equations: those contain velocity and rotor position, do not appear in model resistances and inductances estimation. It can be observed from a set of Equations (3.28) that

coefficients M_1, M_2 and M_3 do not have motor velocity and position variable in them. Resistances and inductances of motor per phase model have been calculated using the same coefficients which are independent of motor velocity and rotor position [16]. The Equation(3.20)

Table 3.1: Characteristic of Parameter Matrix[16].

–	$x_{11} + x_{22}$	$x_{11} - x_{22}$	$x_{12} + x_{21}$	$x_{12} - x_{21}$
I	2	0	0	0
J	0	0	0	-2
$Q(2\Delta\theta_{re})$	0	2cos($2\Delta\theta_{re}$)	2sin($2\Delta\theta_{re}$)	–
$S(2\Delta\theta_{re})$	0	-2sin2($\Delta\theta_{re}$)	2cos($2\Delta\theta_{re}$)	–

represents some of the important matrices which define co-ordinate frame used in parameter identification in [16]. The parameter matrix $\hat{\Theta}(k)$ comprises of four matrices, given as follows:

1. I: represents Identity matrix.

2. J: $\frac{\pi}{2}$-degree rotation.

3. O: Null matrix

4. $Q(2\Delta\theta_{re})$: represents arbitrary points moving in a two-dimensional plane moving symmetrically to the straight line of the θ_{re} radian.

5. $S(2\Delta\theta_{re})$: is a matrix that moves the points symmetrically to the straight line of $\left(\theta_{re} + \frac{\pi}{4}\right)$ radians.

$$I = \begin{bmatrix} 1 & 0 \\ 0 & 1 \end{bmatrix} ; J = \begin{bmatrix} 0 & -1 \\ 1 & 0 \end{bmatrix} ; O = \begin{bmatrix} 0 & 0 \\ 0 & 0 \end{bmatrix} \tag{3.20}$$

$$Q(2\theta_{re}) = \begin{bmatrix} cos(2\theta_{re}) & sin(2\theta_{re}) \\ sin(2\theta_{re}) & -cos(2\theta_{re}) \end{bmatrix} ; S(2\theta_{re}) = \begin{bmatrix} -sin(2\theta_{re}) & cos(2\theta_{re}) \\ cos(2\theta_{re}) & sin(2\theta_{re}) \end{bmatrix}$$

3.4.3 Discrete System

The given below is the discrete form of the extended EMF model presented in [16].

$$\begin{bmatrix} i_{\hat{d}}(n+1) \\ i_{\hat{q}}(n+1) \end{bmatrix} = A \begin{bmatrix} i_{\hat{d}}(n) \\ i_{\hat{q}}(n) \end{bmatrix} + B \begin{bmatrix} v_{\hat{d}}(n) \\ v_{\hat{q}}(n) \end{bmatrix} + C[1] \tag{3.21}$$

$$A = \begin{bmatrix} a_{11} & a_{12} \\ a_{21} & a_{22} \end{bmatrix} \tag{3.22}$$

$$= \frac{-R_s L_o \Delta T_s + L_d L_q}{L_d L_q} I + \frac{R_s L_1 \Delta T_s}{L_d L q} Q(2\Delta\theta_{re}) + \frac{\omega_{re}(L_d^2 + L_q^2)\Delta T_s}{2L_d L_q} J - \frac{\omega_{re}(L_d^2 - L_q^2)\Delta T_s}{2L_d L_q} S(2\Delta\theta_{re})$$

$$B = \begin{bmatrix} b_{11} & b_{12} \\ b_{21} & b_{22} \end{bmatrix} = \frac{L_o \Delta T_s}{L_d L_q} I - \frac{L_{1s}}{L_d L_q} Q(2\Delta\theta_{re})$$

$$C = \begin{bmatrix} c_1 \\ c_2 \end{bmatrix} = \frac{\omega_{re} K_e \Delta T_s}{Lq} \begin{bmatrix} sin(\Delta\theta_{re}) \\ -cos(\Delta\theta_{re}) \end{bmatrix}$$

$$\mathcal{Y} = \Theta Z \tag{3.23}$$

Θ in the Equation(3.23) is a parameter matrix that can be determined using the ***Recursive Least Method*** , given in Equations (3.26) and (3.27), for known $\mathcal{Y}$ and Z as follows in Equation(3.24):

$$\mathcal{Y} = \begin{bmatrix} \hat{i}_d(n+1) & \hat{i}_q(n+1) \end{bmatrix}^T \tag{3.24}$$

$$Z = \begin{bmatrix} \hat{i}_d(n) & \hat{i}_q(n) & \hat{v}_d(n) & \hat{v}_q(n) & 1 \end{bmatrix}^T$$

$$\Theta = \begin{bmatrix} A & B & C \end{bmatrix} = \begin{bmatrix} a_{11} & a_{12} & b_{11} & b_{12} & c_1 \\ a_{21} & a_{22} & b_{21} & b_{22} & c_2 \end{bmatrix}$$

$$\varepsilon_i = (\mathcal{Y} - \hat{\Theta}Z)^2 \tag{3.25}$$

$$\hat{\Theta}(k) = \Theta(k-1) + (\mathcal{Y} - \Theta(k-1)Z)Z^T P(k) \tag{3.26}$$

$$P(k) = \frac{1}{\lambda}\left(P(k-1) - P(k-1)Z(\lambda + Z^T P(k-1)Z)^{-1} \times Z^T P(k-1)\right) \tag{3.27}$$

The motor parameters can be determined by using recursive least square (RLS) in Equations (3.26) and (3.27) with the '*Characteristic Matrix*', given in the Table (3.1) compare to using Equation (3.22) directly as it contains velocity and rotor position. Using Table (3.1) simplifies the relations as follow:

$$M_1 = b_{11} + b_{22} = \frac{2L_o\Delta T_s}{L_d L_q} \tag{3.28}$$

$$M_2 = a_{11} + a_{22} - 2 = -2\frac{RL_o\Delta T_s}{L_d L_q}$$

$$M_3 = \sqrt{(b_{11} - b_{22})^2 + (b_{12} - b_{21})^2} = -2\frac{L_1\Delta T_s}{L_d L_q}$$

From Equation (3.22) BLDC motor parameters can be estimated as follows:

$$\hat{R} = |-\frac{M_2}{M_1}| \tag{3.29}$$

$$\hat{L}_d = |\frac{2\Delta T_s}{M_1 + M_3}|$$

$$\hat{L}_q = |\frac{2\Delta T_s}{M_1 - M_3}|$$

Least Mean Square (LMS) estimate motor parameters along with the error estimation, using the low pass filtered line currents and phase to phase voltages. Once dynamic parameters are identified then motor velocity can be estimated by applying the observer. Motor velocity and rotor position deviate from their reference the same degree as the estimated error in process of parameter identification.

3.4.4 Minimal Order State Observer to Estimate Extended EMF

Equation (3.30), taken from [16], is the minimal state observer which estimate the stationary frame current and Extended EMF.

$$\dot{\hat{i}} = A_{11}i + A_{12}\hat{e} + B_1 v \tag{3.30}$$

$$\dot{\hat{e}} = A_{11}Gi + (A_{22} + A_{12}G)\hat{e} + B_1 Gv - G\dot{i}$$

$$\hat{\theta}_{re} = tan^{-1}\frac{\hat{e}_\alpha}{\hat{e}_\beta} \tag{3.31}$$

3.5 Linear Quadratic Regulation

The LQR algorithm is known for its an automated way of finding an appropriate state-feedback controller. The linear quadratic regulator (LQR) calculates optimal gain matrix (K) for a continuous time system e.g., in our case we are trying to improve the observer response. The extended EMF is a parameter estimation based strategy. It's response time is 2 ms, which is need to be expedited for improved results. A LQR based controller follows the state feedback law $U = -Kx$, that reduces the cost function Index given by the Equation (3.32).

$$J_c(U) = \int_0^\infty \left(x^T Q_c x + U^T R_c U + 2x^T N_c U\right) dt \tag{3.32}$$

Where x is represents the state of a linear time invariant state space system and U is the applied input. The matrices, Q_c, 'R_c', and N_c are 2×2 in size for two input and two output system. By increasing weight on $Q_c(1,1)$ improves rise time of the system and on $Q_c(2,2)$ tunes the settling time. The matrix R_c is taken as Identity matrix and 'pre-compensation means to rescale the gain matrix to force N_c reduces the steady state error to zero. The LQR based system response improvement is better compensation compare to pole place method of response improvement as hence found gain always keep system stable and controllable[4].

3.6 Summary

This chapter is concise information about fundamental motor principle of operations. There are different types of the synchronous motors which could be single salient or double salient. A slight change of the type of motor require a different model for its actual behaviour emulation. The mathematical modelling of BLDC motors using electrical, magnetic and electromechanical properties is presented. The magnetic model of the BLDC motors can be constructed using the fundamental principles of electromagnetics that involve the magnetic properties of the BLDC motors such as magneto motive force (MMF). We selected a motor model that is well suited for most of the synchronous motors. This model has terms which contain motor rotor position information. That's why this model can be a good selection in the research of a rotor position estimation using motor model by identifying its parameters. A brief understanding has been developed in this chapter for the extended EMF based motor modelling. An improvement in the extended EMF model has been made using a least quadratic regulator controller. The improvement in the model ensures a fast and stable model response. As in this approach parameters vary due to varying load on the motor shaft, temperature and magnetic saturation.

Chapter 4

Experimentation and Applied Strategies

This thesis presents a combination of in lab instrumentation, computer-based data acquisition, and measurement in order to test and implement the sensorless schemes for BLDC motors. A series of experiments were executed to estimate a sensorless model for high power BLDC motor. The main contribution of this thesis is the off-line impedance measurement of BLDC motor using LCR meter and per phase motor model development with it. The second contribution is improving the observer of the applied sensorless strategy, the extended EMF model which estimates the rotor position of the motor using its voltage and current signals.

The motor per phase model is rotor position dependent which is based on the phase impedance measurement for a wide range of frequencies. The proposed motor model well imitates the parameters associated to permanent-magnet synchronous motors. The same model is needed to be upgraded for an on-line parameter motor model by utilizing high frequency input/output inverter signal's harmonics. In order to estimate an equivalent motor model with internal model principle, the two fundamental pieces of information are required: 1) An access to motor winding neutral point, 2) a good approximate estimation of an equivalent model for the motor. The second piece of information provides for position estimation via a real-time Fourier series representation of the measured voltage and current produced by the IMP algorithm. With this the data can be fit to the appropriate θ_{re} dependent model and θ_{re} can be determined.

4.1 Experimentation

We conducted two types of data acquisition experiment arrangements to estimate rotor po-
sition dependent motor model under observation i.e., the off-line impedance measurement
and computer-based data acquisition. The off-line motor phase impedance had simply been
measured by using the regular low frequency and high frequency LCR meters. For an on-line
motor parameter identification, a data acquisition card, a voltage divider circuit and two Hall
effect sensors had been attached to provide computer-based motor phase voltage and current
measurement. The on-line data acquisition of the motor phase to phase voltages and phase
currents have been recorded in motor stalled torque experiment. Moreover, motor voltage and
current signals were also recorded for no load and certain load configurations.

4.1.1 The Off-line Impedance Measurement

A LCR meter is a device, used to measure resistance (R), inductance (L) and capacitance (C) of
motors and transformers' windings, power connecting cords, and communication cables
etc. The Table(4.1) shows the impedance values recorded for series and parallel LCR meter
modes for maximum, minimum and intermediate impedance points on motor positions. The
symbol "zs" denotes the series equivalent model impedance and 'zp' denotes the parallel
equivalent model impedance of motor windings.   Usually device under test (DUT) is sub-

Table 4.1: Phase AB impedance measurement for maximum, medium, and minimum induc-
tance rotor positions.

Freq kHz	0.1	1	10	75	103
zs_{max} Ω	0.61+j1.1	1+j10.8	19.7+j96.5	800+j441	924+j539
zp_{max} Ω	1.6 -j 0.3	0.46 - j0.49	0.05 - j2E-4	0.8E-03 -j 0.5E-03	0.8E-03 - j0.5E-3
θ_s	61°	84.7°	78.5°	28.9°	30.3°
zs_{med} Ω	0.6+j1.04	0.95+j10	17.4+j9E01	720+j67.8	825+j448
zp_{med} Ω	1.5-j0.27	0.46-j0.5	0.041-j0.02	1E-3 - j6E-4	9E-4 - j5E-4
θ_s	60.8°	84.5°	79°	27.1°	28.5°
zs_{min} Ω	0.61+j9.6E-1	0.92+j9.3E	15.5+j8.4E1	723+j3.7E2	826+j447
zp_{min} Ω	1.6-j0.3	0.5 - j0.51	4.23E-2 - j2.12E-2	1.1E-3 - j6E-4	9E-4 - j5E-4
θ_s	57.7°	84.4°	79.6°	26.9°	28.4°
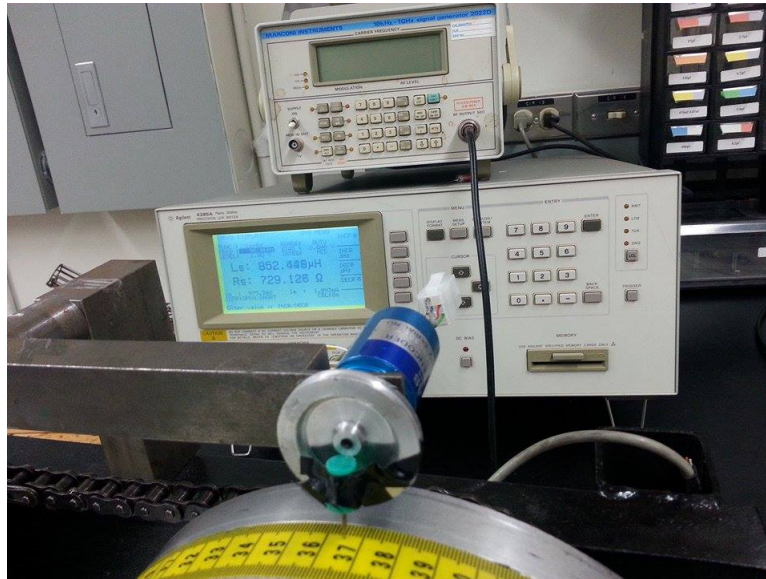
Figure 4.1: The BLDC motor phase AB resistance and inductance Measurement at different frequencies above 75 kHz with LCR meter (Agilent 4285A).

jected to an ac voltage source of adjustable frequency in *Hz*. Note that the hand held LCR meter e.g., BK Precision (879) has frequency range as 10, 100, 1000 and 1 kHz and Agilent (4285A) LCR has measuring range from 75 kHz to up to 30 MHz Therefore, in order to measure the frequency for both low and high frequency we had to use both types of meters. The device measures the voltage and current across the DUT and calculates impedance with the ratio of their magnitudes and the phase between them. The impedance for maximum, medium and minimum points on the rotor are given in table above for different frequencies between 100 to 103 kHz. By examining the impedance reading we can conclude that the relationship of these impedance points with increasing frequencies is not linear, indicating that the circuit is not a simple parallel or series model.

4.1.2 The Computer-based On-line Data Acquisition

The Figure (4.1.2) is a block diagram of our experimental data acquisition configuration. We labelled motor phases as follows:A, B and C. A short review of each block in this block

diagram is given in proper sequence as follows:
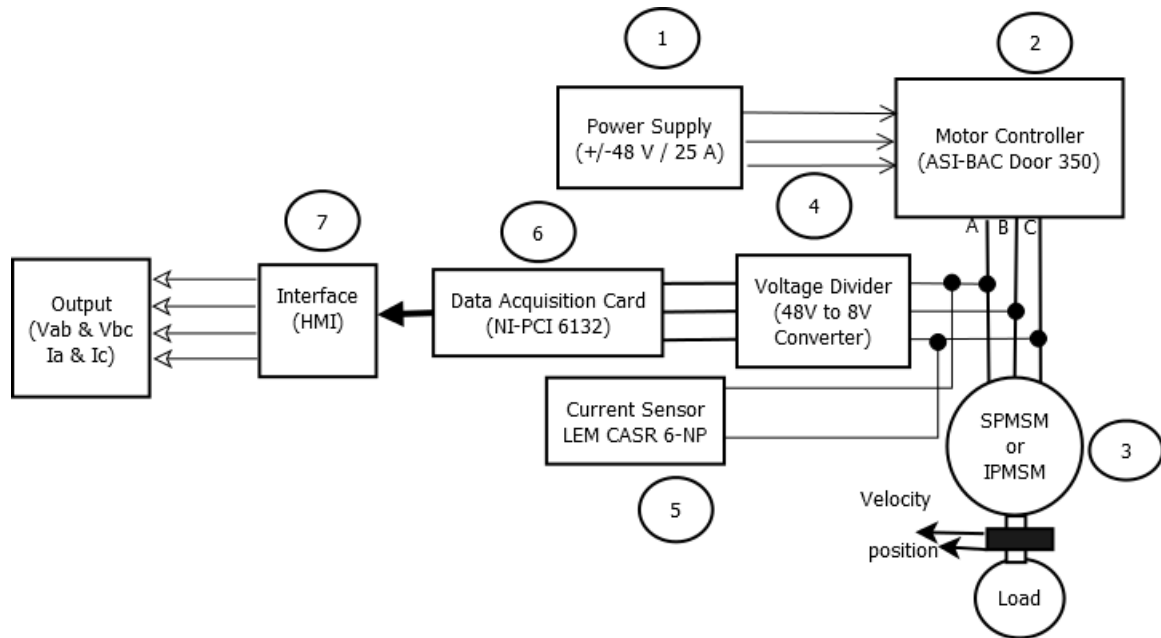
Figure 4.2: On-line data acquisition block diagram.

1. The block number 1 is a $\pm 48\,\text{V}/25\,\text{A}$ power supply.

2. The block number 2 is a ASI BAC Door 350 motor controller. The motors which are controlled by the controllers (BAC Door 350), are used for high power density speed and torque control applications for various electric vehicles.

3. The block number 3 represents the brushless DC motors e.g., surface permanent- magnet motor or an interior permanent-magnet motor with an optional load.

4. The block number 4 is a voltage divider circuit that scales the motor phase to phase $\pm 48\,\text{V}$ into it's $\frac{1}{6}$ the fraction according to NI-PCI 6132 data acquisition board specification. The NI-PCI 6132 board in the block number 6, has has 4 analog differential inputs [28].

5. The block number 5 is a Hall sensor (LEM CASR 6-NP) and it's output is a relative voltage (v_{out} in 'V') to a calibrated range of current. In order to get the current in units

of amperes, we need to divide the signal by given theoretical sensitivity (Gth) which is $625\,\text{mV}/I_{PN}$ (where I_{PN} is the primary nominal current of $2\,\text{A}$). The theoretical sensitivity is given in [29] in the electrical data table for current sensor.
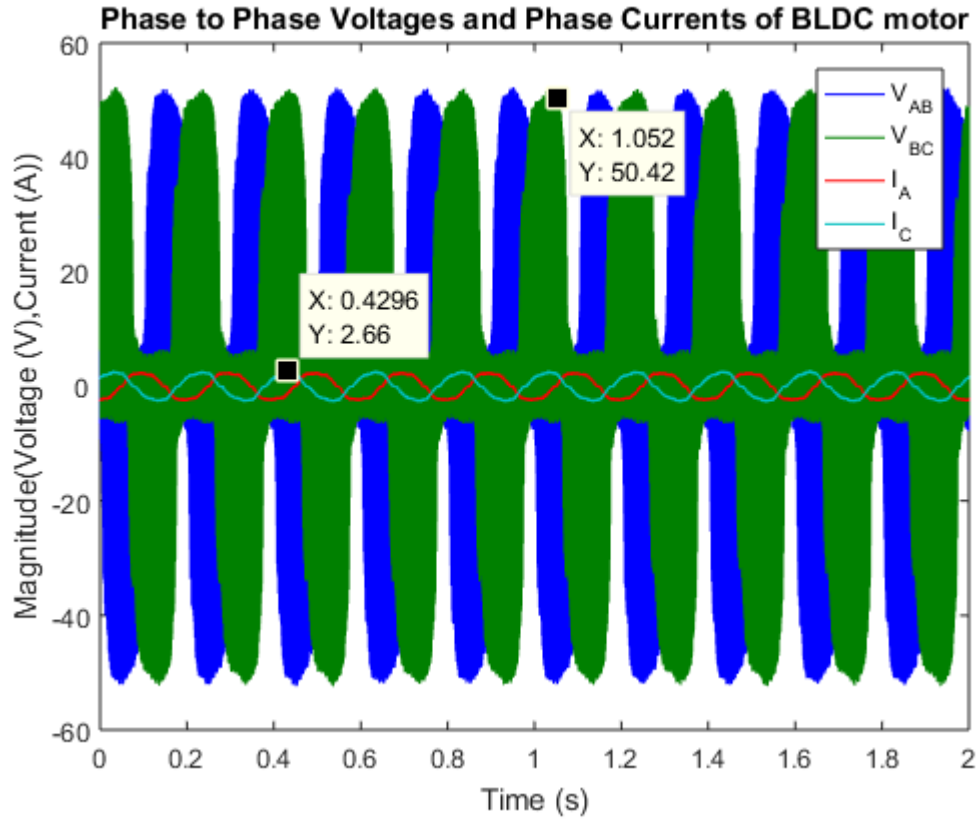
Figure 4.3: BLDC motor's input in voltages in (V) and output of current sensor in (A) for no load experiment.

The output of this experimental set up, (i.e., given in Figures (4.3) and 4.4), which comprise of the phase to phase BLDC motor voltage inputs, V_{AB} and V_{BC}, and output current phase currents I_A and I_C. The sampling rate of this data collection is $1\,\text{MHz}$ and switching frequency of the inverter is $13\,\text{kHz}$.

The Figure(4.3) represents the motor phase to phase voltages(i.e., V_{AB} and V_{BC} in (V)) and phase current(i.e., I_A and I_C in (A)), for no load experimentation. The voltage deviates within the range $\pm48\,\text{V}$. The peak to peak current of magnitude $5\,\text{A}$ for synchronous
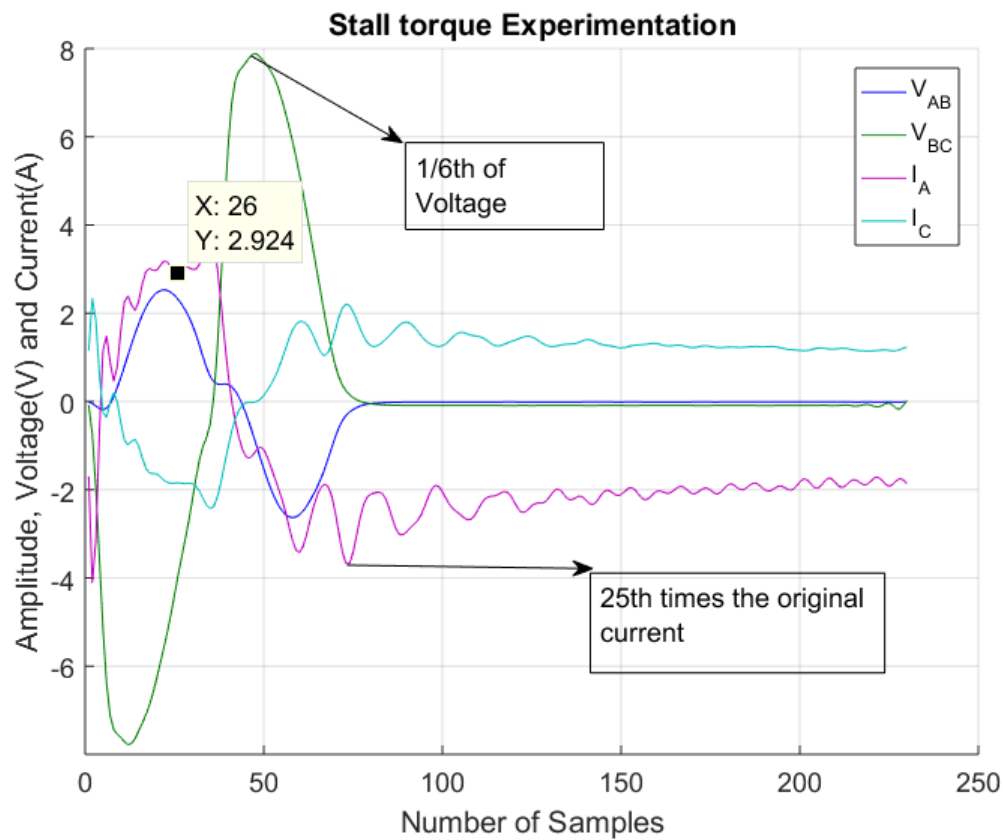
Figure 4.4: BLDC motor's input in voltages in (V) and output of current sensor in (A) for stall torque experiment.

reference speed of 5 Hz. The three phase motor power signals are approximately 120° from each other. On the other hand, the Figure (4.4) shows the computer based data acquisition for stalled torque experiment. This figure contains only one cycle of the stall data the overall voltage and current signals are given by Figures (5.4) and (5.5), which have been measured in stall torque experiment. The current obtained in stall experiment set up was less in magnitude therefore current had to scaled for better understanding of current shape. For this part of the experimentation, the motor had been stalled for the maximum inductance and minimum inductance rotor position. This piece of information provides a distinct view of controller's commutation scheme for the stalled torque condition. In this case, the Back-EMF of motor becomes zero due to motionless rotor. Therefore, the recorded voltages and currents' infor-

mation can vividly be used to measure the on-line impedance of motor winding. The phase current in this experimentation is very low due to excessive power dissipation due to copper losses.

4.2 The Applied Strategies

The two methods have been used to determine a suitable equivalent motor model. These are the **off-line** impedance based motor model and on-line impedance based motor model.

In off-line strategy, a motor model has been proposed that well explains the direct and quadrature inductances (L_d and L_q) for permanent-magnet motor model. This model is designed to imitate the actual parameter variation of the motor model. The sensorless operation of permanent-magnet motor can well be explained by using this model and can replace the position sensors in motors. On the other hand, the **on-line** sensorless motor model methods have been applied using **the internal model principle** and **the extended EMF model**. The internal model principle based motor model can determine the dynamic behaviour of the motor model. In this strategy, the high energy harmonics of the power signals are used to calculate the coefficients of the desired motor model. Last but not least is the **extended EMF** based motor model. This sensorless motor model is based on the parameter identification theory and an observer calculates the extended EMF from motor voltage and current signals in real time. The rotor position and angular speed are continuously being updated in the system. Therefore, at each instance the stationary frame extended EMF pair (e_α, e_β) and phase between these signals can detect a better rotor position estimate.

The theory behind the applied strategies has briefly explained in this section and their implementation and results will be shown in next chapter.

4.2.1 The Off-line Motor Model Using Least Mean Square

The electrical properties of permanent- magnet DC motors depend upon the following parameters: e.g., the motor current, voltage, flux linkage, Back-EMF, and motor winding coils. The

Figure(3.2) is a commonly used BLDC model, which in our case requires improvement, because the inductance of permanent-magnet motor under observation varies with respect to rotor position.

The reluctance is a magnetic resistance in magnetic circuits and has a converse correspondence to inductance.

The inductance in BLDC motor's winding varies due to air gaps within the motor rotor and stator. The DQO-transform is a representation of magnetic as well as electrical properties of the BLDC motor. Our proposed model for BLDC motor in the Figure (4.5) has a resistance in series with inductance that represents the motor winding and another resistor in parallel with inductor for iron losses.
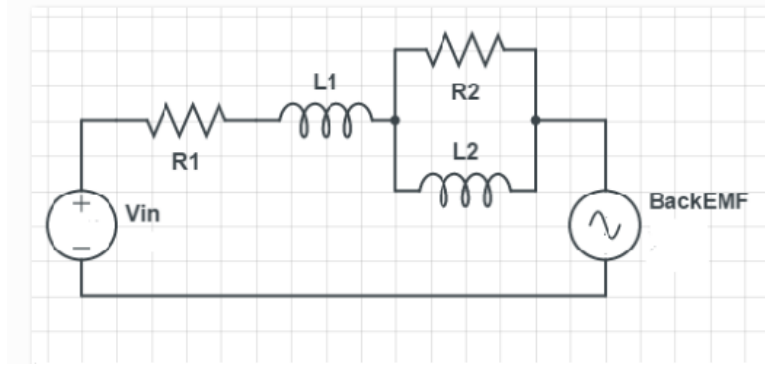
Figure 4.5: The proposed BLDC motor per phase model.

$$Z(s) = \frac{L_1 s^2 + as + b}{s + c} = \frac{L_1 s^2 + (R_2 L_1/L_2 + R_1 + R_2)s + R_1 R_2/L_2}{s + R_2/L_2} \qquad (4.1)$$

Equation (4.1) is the transfer function of the phase to phase impedance of the circuit in Figure (4.5). The model coefficients, the rotor position dependent motor model's resistances and inductances, can be estimated using the measured impedance points in the Table(4.1). L_1, a, b and c can be found using least squares fitting and from these the following formulas give the impedances and resistances.

$$R_1 = \frac{b}{p}$$

$$R_2 = a - L_1 p - R_1$$

$$L_2 = \frac{R_2}{p}$$

To set up the least squares problem, rewrite Equation (4.1) as

$$j\omega Z = \begin{bmatrix} L_1 & a & b & c \end{bmatrix} \times \begin{bmatrix} -\omega^2 \\ j\omega \\ 1 \\ -Z \end{bmatrix} \tag{4.2}$$

Separating into real and imaginary components gives

$$-\omega * I_m Z = \begin{bmatrix} L_1 & a & b & c \end{bmatrix} \times \begin{bmatrix} -\omega^2 \\ 0 \\ 1 \\ -R_e Z \end{bmatrix}$$

$$\omega * R_e Z = \begin{bmatrix} L_1 & a & b & c \end{bmatrix} \times \begin{bmatrix} 0 \\ \omega \\ 0 \\ -I_m Z \end{bmatrix}$$

$$\Phi = \begin{bmatrix} I_m Z_{\omega_1} \\ R_e Z_{\omega_1} \\ I_m Z_{\omega_2} \\ . \\ . \\ . \\ R_e Z_{\omega-n} \end{bmatrix}_{n \times 1} \quad ; \Theta = \begin{bmatrix} -\omega_1^2 & 0 & 1 & -R_e Z_{\omega_1} \\ 0 & \omega_1 & 1 & -I_m Z_{\omega_1} \\ -\omega_2^2 & 0 & 1 & -R_e Z_{\omega_2} \\ . & . & . & . \\ . & . & . & . \\ 0 & \omega_n & 1 & -I_m Z_{\omega_n} \end{bmatrix}_{n \times 4} \tag{4.3}$$

$$\begin{bmatrix} \hat{L_1} \\ a \\ b \\ c \end{bmatrix}_{Y} = \underbrace{W\left(\Theta^T\Theta\right)^{-1}\Theta^T}_{X} \times \Phi \tag{4.4}$$

Where W is a diagonal weighting function to compensate for the changing magnitude of the impedances. Figure(5.2) is the percent error of the weighted least mean square estimator (LMS), given in chapter(5).

4.2.2   The Internal Model Principle Strategy

The internal model principle (IMP) was proposed by B.A.Francis and W.M.Wonham in year 1976 [30]. According to this principle if the input disturbance $u(t)$, output disturbance E_o or a reference $S(t)$ has generating polynomial, $\Gamma_d(s)$, then a controller of form in Equation (4.5) with standard error feedback control architecture can asymptotically reject the effect of the disturbance and it's output tracks the reference. In model implementation, only disturbance causing polynomials are required, the disturbance magnitude and relative phase are not needed.

$$C(s) = \frac{P(s)}{\Gamma_d(s)} \tag{4.5}$$

In Figure(4.6), $L(s)$ is the tuning function, x is IMP states matrix, u_h is the total sum of extracted harmonics.In IMP controller design $P(s)$ and $\Gamma_d(s)$ are selected arbitrary such that the characteristic equation has eigenvalues with negative real parts.

4.2.3   The Harmonics Extraction Using IMP

Harmonics of a time varying sinusoidal power come into existence due to multiple reasons such as non-linear loads, switching frequency of the controller or power supplies in AC/DC motors, rectifiers and electric arc furnaces etc. These harmonics contain energy and drive non-sinusoidal current from a sinusoidal electric power source [31].
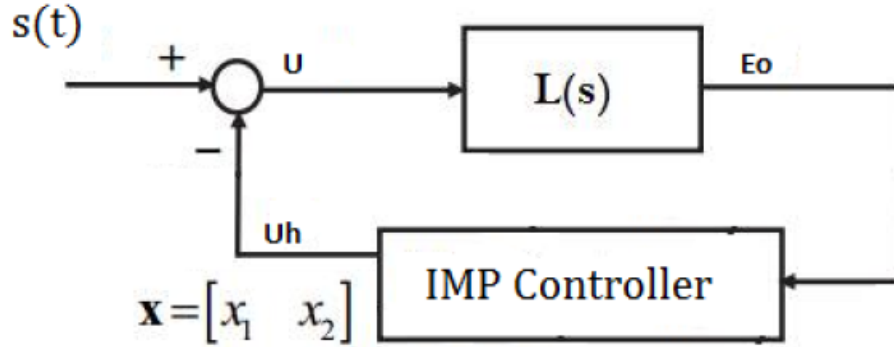
Figure 4.6: Block diagram of adaptive internal model principle based control system.

The Internal Model Principle algorithm is an alternative tool of instantaneous Fourier Series. The noise components of power signals of the system automatically bypass using IMP. The pulse width modulated power signals of the system can be represented as the sum of its fundamental frequency component and associated harmonics, as follows:

$$s(t) = \sum_{i=1, 2, 3, \cdots} A_i cos(\omega_i t + \phi_i) \tag{4.6}$$

where A_i, and ϕ_i are the magnitude, and initial phase of the ith harmonic respectively and ω_i is the pulse width modulation frequency. Note that (A) will be a periodic signal with period equal to the electrical frequency of the motor.

The Equation (4.7) is a state space representation for i^{th} harmonic internal model principle controller. This model has two states: x_1 and x_2. For an on-line impedance motor phase model, the magnitude and relative phase between model states are required for high energy harmonics. The harmonics' magnitude and related phase can be calculated by using the Equation (4.8).

$$\begin{bmatrix} \dot{x}_i \\ \dot{x}_i \end{bmatrix} = \begin{bmatrix} 0 & \omega_i \\ -\omega_i & 0 \end{bmatrix} \begin{bmatrix} x_1 \\ x_2 \end{bmatrix} + \begin{bmatrix} 0 \\ 1 \end{bmatrix} s \tag{4.7}$$

$$u_i = \begin{bmatrix} K_1 & K_2 \end{bmatrix} \begin{bmatrix} x_1 \\ x_2 \end{bmatrix}$$

Magnitude M_i and Phase ϕ_i of a discrete harmonic ($i = 0, 1, 2, 3 \cdots$) can be extracted using the following expressions:

$$M_i = \sqrt{(K_{1i}^2 + K_{2i}^2)} \sqrt{(x_{1i}^2 + x_{2i}^2)} \tag{4.8}$$

$$\phi_i = tan^{-1}\left(\frac{x_{1i}(t)}{x_{2i}(t)}\right)$$

We are interested in estimating an equivalent BLDC motor per phase impedance model using high energy power signal harmonics. In permanent-magnet motors there are air gaps between rotor and stator poles due to rotor magnet grooves. Thus the motors have time varying position dependent inductance due to varying flux linking of motor poles during rotation.

The internal model principle algorithm has been applied on the measured power signals of the motor, voltage and currents. In order to generate instantaneous Fourier series representations of these signals. The ratios of the coefficients of these two series give the motor impedances at the switching frequency at its harmonics. The PWM signals were acquired for two inductance based rotor positions, "**Maximum Inductance** and **Minimum Inductance**".

Let the residual of the algorithm be the difference between the measured signal and estimated Fourier series representation of the signal. The bode plot of the transfer function from the signal being analyzed to residual is given in Figure(4.7). The step response is given in Figure (4.8). Note the residual decays in about in $\frac{1}{10}^{th}$ of signal time period. The estimated signal can be constructed as the cumulative sum of multi IMP models in the feedback of the tuning function $L(s)$.

$$T_{bp}(s) = \frac{1.10BW^2 s^2}{s^4 + c_1 s^3 + c_2 s^2 + c_3 s + c_4} \tag{4.9}$$

$$c_1 = 1.1BW$$

$$c_2 = 2\omega_o^2 + 1.1BW^2$$

$$c_3 = 1.098\omega_o^2 BW$$

$$c_4 = \omega_o^4$$

$$T_{bpn}(s) = \frac{1.10BW^2 s^2}{s^4 + c_1 s^3 + c_2 s^2 + c_3 s + c_4} \prod_{i=1}^{n} \frac{s^2 + \omega_i^2}{s^2 + 2\varepsilon_i \omega_i + \omega_i^2} \tag{4.10}$$
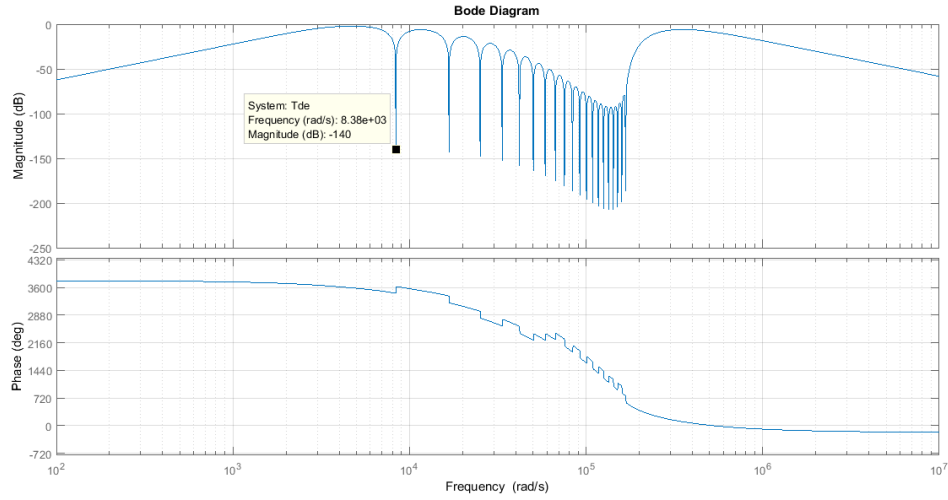
Figure 4.7: The internal model design for BLDC motor harmonics extraction using notch filters.

In order to ideally identifying the desired T_{bpn}, the tuning function must have the transfer function $L(s) = \frac{M(s)}{N(s)} = \frac{b1s^2}{s^4 + a_1 s^3 + a_2 s^2 + a_3 s + a_4}$ and IM transfer function $\frac{K_{2i}s + K_{1i}}{s^2 +}$ in the feedback with $L(s)$. Since, L(s) with N number of IMP modules in feedback to form $T_{de}(s)$ as follow:

$$T_{de}(s) = \frac{L(s)}{1 + L(s) \sum_{i=1}^{n} \left(\frac{K_{2i}s + K_{1i}\omega_i}{s^2 + \omega^2 i^2}\right)} \tag{4.11}$$

$$= \frac{M(s) \prod_{i=1}^{n}(s^2 + \omega i^2)}{N(s) \prod_{i=1}^{n}(s^2 + \omega i^2) + M(s)D(s)}$$

Table 4.2: Coefficient Calculation for Tuning Function $L(s)$.

b1	a1	a2	a3	a4
1.34E+03	87.38	3.95E+03	708.17	163.21

Table 4.3: Coefficient Calculation for $D(s)$.

–	$K_{1,i}$	$K_{2,i}$	$K_{1,i+1}$	$K_{2,i+1}$	$K_{1,i+2}$	$K_{2,i+2}$
i=1	0.02	0.08	-0.045	0.16	-0.14	0.22
i=4	-0.24	0.26	-0.36	0.28	-0.49	0.3
i=7	-0.62	0.31	-0.78	0.32	-0.94	0.34
i=10	-1.13	0.36	-1.34	0.4	-1.6	0.46
i=13	-1.84	0.55	-2.14	0.69	-2.46	0.89
i=16	-2.81	1.17	-3.17	1.58	-3.54	2.11
i=19	-3.78	2.84	-4.07	3.78	-3.87	4.92
i=22	-3.73	6.43	-2.49	7.86	-1.01	9.57
i=25	2.02	10.54	5.83	10.47	10.4	7.78
i=28	13.26	1.43	9.76	-7.09	-1.05	-7.32
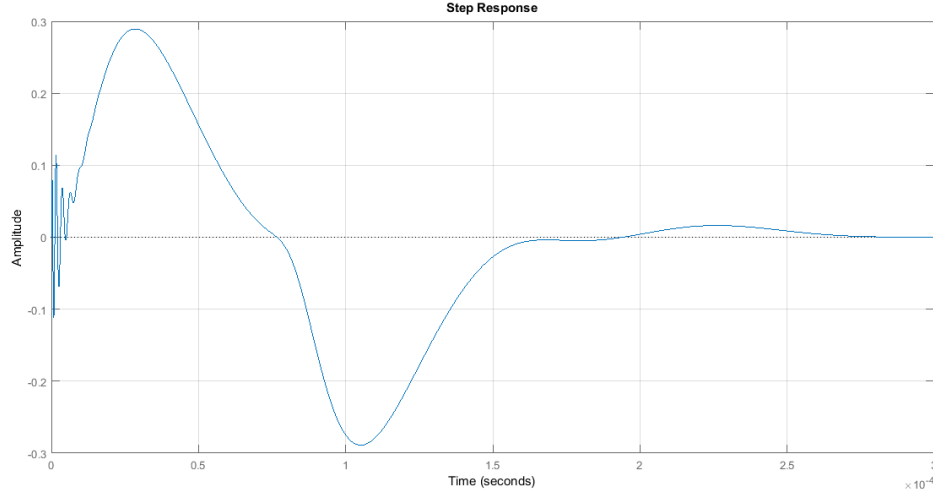
Figure 4.8: IMP algorithm step response.

Where, $D\big(s\big) \;=\; \sum_{i=1}^{n}\Big((K_{2i}s \,+\, K_{1i}\omega i)\prod_{l=1,n}^{l\neq i}(s^2 \,+\, \omega_l^2)\Big).$ The Tables (4.2 , 4.3) are the numerical values of the calculated coefficients for the tuning function $L(s)$ and gain for $D(s)$ coefficients.

In summary, the internal model principle is an alternative tool to Fast Fourier transform for frequency response analysis of the quasi periodic signals. The algorithm is implemented such that the transfer function from the signal to be analysed to the residual is a bandpass filter cascaded with a notch filter. Ideally, $T_{de}(s)$ output response must be zero or converge to zero in short duration of time, for perfect system identification. The wider the width of the notch filter at the desired location of the harmonic frequency, the higher the leakage frequency and longer it takes for estimator to acquire steady state response. Narrower the notch width lesser the leakage frequency, lesser the settling response time and reduces DC-offset considerably but there is the chance to miss the fundamental frequency. With the help of IMP based frequency response of the motor phase exciting voltages and current dynamic

motor impedance model can be developed.

4.2.4   The Extended EMF Model Strategy

Ichikawa et al. (2006) presented a sensorless speed control for permanent- magnet synchronous motors based on on-line parameter identification theory. The extended EMF based rotor position estimation is independent of high frequency signal injection that is used for motor parameter identification. The signal injection makes the extended EMF model suitable for low speed and near standstill. The rotor position and motor system parameters continuously update in motor model observer during the operation. This strategy has a continuous feed of motor parameters in loop therefore, this model is sensitive to parameter variation. The model observer estimates the extended EMF ($\hat{e}_\alpha$, $\hat{e}_\beta$) on a stationary reference frame, where the phase between the extended EMF coordinates estimate the rotor position. The extended EMF is a combination of Back-EMF and motor saliency due to rotor permanent-magnets. The extended EMF stationary frame coordinate phase is equivalent to the estimated rotor position. The motor parameters deviate due to load on the motor shaft. As the load on the motor shaft increases, the motor exerts more power to maintain it's persistent rotations per minute. After this variation in the load, the actual values of parameters are regained after a time lapse of estimator's response time.

The extended EMF model is one of the efficient models for dynamic model parameter identification for all types of synchronous motors. The stator winding current is sensed using Hall effect sensor and then converted from analogue to digital signal processor (A/D) by a high speed DSP-processor (DSP TMS320VC33), FPGAs etc. After analogue to digital conversion, the three phase motor currents and input voltages in the first step are transformed into two phase signals on the stationary reference frame signals. In the second stage, these signals are transformed into the estimated rotating frame signals as shown in Figure (2.14) of chapter (2) of this thesis. The observer estimates the motor rotor position and velocity with an on-line motor parameter identification.

By inferring from the explanation of the extended EMF given by Ichikawa et al. (2006)

and Morimoto *et al.* (2001), some of the rudimentary aspects about the suitability of the *extended EMF* for synchronous motors have been concluded as follows: The extended EMF error ($\Delta\theta_{re}$) increases in direct proportion with the growing differences between actual motor parameters and estimated parameters. These difference are the result of internal and external temperature of motors and their deviating magnetic saturation with varying load [16].
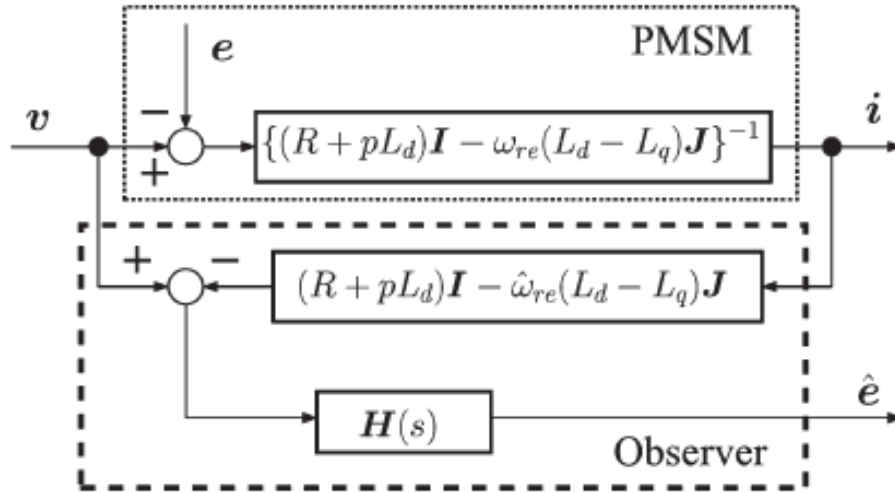
Figure 4.9: Extended EMF based Observer[16].

The synchronous motors are classified into three types 1) surface PMSM 2) Interior PMSM and 3) switched reluctance motors (SRMs) based on their rotor position dependent stator direct (L_d) and quadrature (L_q) inductances. PMSM ($L_d = L_q$), interior PMSM ($L_d < L_q$) and synchronous reluctance motor ψ_a magnetic flux linkage is zero [32].

4.2.5 Parameter Identification

The extended EMF based sensorless rotor estimation is one of the most efficient rotor position estimation methods. The extended EMF utilizes the phase voltages and stator currents information only to estimate rotor position in electrical degrees. In the first step, the recursive least square estimator (RLS) identifies motor stator resistance and rotating frame inductances with low pass rotating frame voltages and currents using the extended EMF model given by

the Equation (3.18). The motor parameters such as stator resistance (R_s), direct magnetic inductance (L_d) deviate from their actual reference point due to temperature, permanent-magnet strength, deviation in power losses, rotor type (e.g., round rotor and salient round rotor), symmetry, and magnetic saturation. The Figure(4.10) shows the results of the applied extended
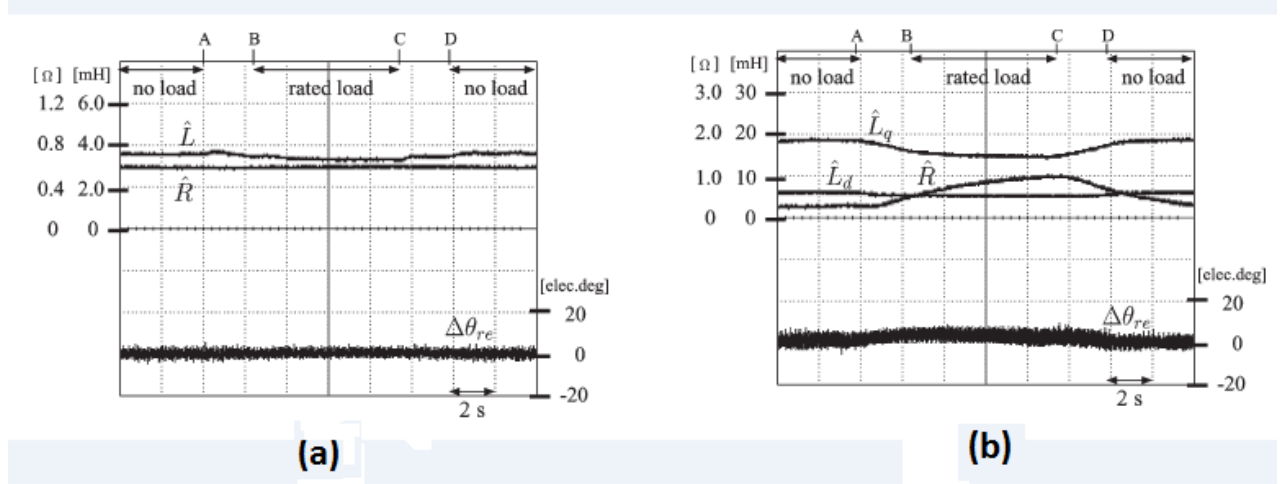
Figure 4.10: a)The parameter identification of surface PMSM at variable load. b)The parameter identification of interior PMSM at variable load. The figure has been taken from [16] with permission.

EMF model on the surface permanent-magnet synchronous motor (SPMSM) and interior permanent-magnet synchronous motor (IPMSM) at 500 rpm by applying the Ichikawa model in section (3.4.3). The estimated stator resistance $\hat{R}_s$ changed from $0.3\,\Omega$ to $1.1\,\Omega$, similarly, $\hat{L}_q$ reduced from 18 mH to 14 mH from no load to rated load condition. The stator resistor and inductor vary with load change as electric power consumption increase so does the losses.

4.3   Summary

This chapter is a brief summary of the experimentation and fundamental understanding of the applied strategies. The two types of experimentation were executed in our lab. The first

is an off-line motor winding resistance and inductance measurement for three different rotor positions. The second is an on-line motor input voltages and output current acquisition with a special data acquisition set up. There are three strategies, which have been implemented on the measured data. The strategies are as follows: we proposed a new rotor position dependent per phase motor model using off-line impedance measurement. Another on-line strategy was partially applied to estimate the rotor position with an on-line method. Last but not the least, the extended EMF model was applied with an improvement in its observer.

Chapter 5

Data Analysis and Result Discussion

In this chapter, a brief data analysis of the applied strategies, for sensorless BLDC motor rotor position dependent models, has been discussed. The challenges during the implementation of these strategies have been highlighted. The two main ways of sensorless motor rotor position estimation have been given in this thesis: those are **off-line** impedance based and position dependent motor model using least mean square and an **on-line** impedance measurement based motor model has been given using **internal model principle** and another on-line motor model has been implemented using the **extended EMF** method. The extended EMF based model is based on the identification theory of parameter estimation. The theory and experimentation of these applied strategies have been given in chapter(4) of this thesis.

5.1 An Off-line Motor Model Estimation using LMS

The Figure (5.1) is a **frequency response** of the magnitude and phase of the actual measured impedance points vs estimated model. Whereas the Figure (5.2) represents the estimation error which converges to zero. The %error of the estimation is a trust tool to validate model accuracy, it needs to be minimum or close to zero for good model parameter estimation. The Table (5.1) is model parameter estimation results.

The frequency response of the proposed model clearly fits the actual motor impedance

points. This is the LMS based coefficient estimation for the proposed model applied on the six measured points. Earlier we selected only five points between the frequency range 100 Hz to 103 kHz but results were not according to the predicted model. As model failed to model behaviour of data at high frequencies. In particular, the identified 2nd zero was non minimum phase, resulting in an increase of the slope of the phase curve when experimental data showed a consistent decrease in this slope. This was rectified by measuring the impedance at 200 kHz and redoing the curve fitting algorithm. With this new data, we got proper matching of the high frequency data.
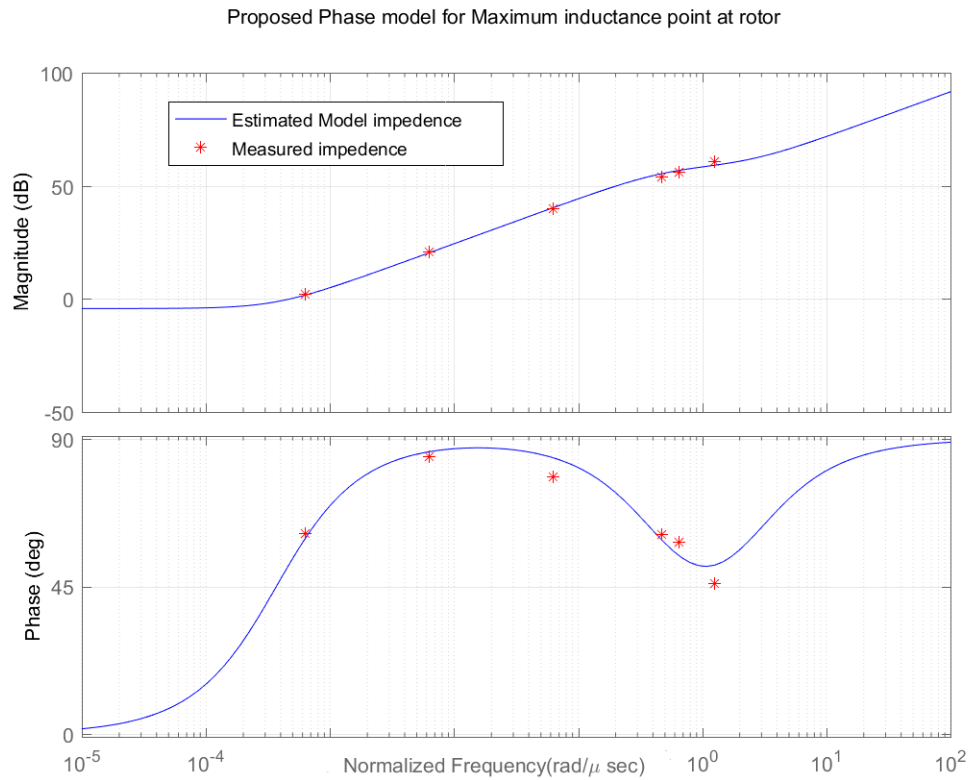

Figure 5.1: Proposed model frequency response vs measured impedance points.

The Figure (5.2) is the percent error of the weighted least mean square estimator (LMS), given in chapter(5).

The Table (5.1) contains the estimated parameters of the proposed model, given in sec-
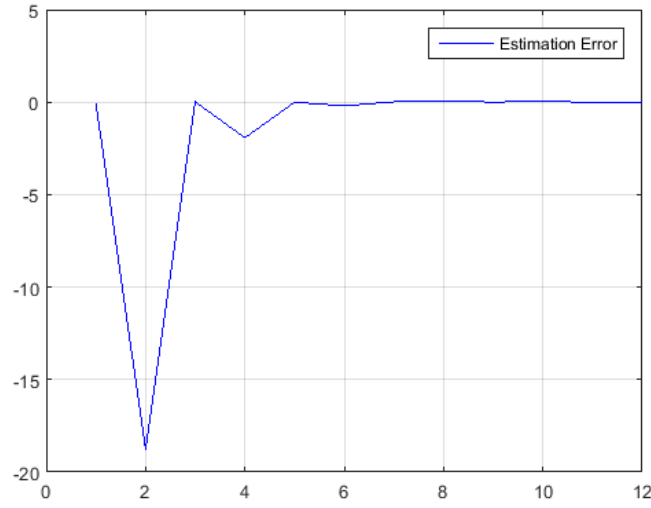
Figure 5.2: Least mean square based parameter estimation error.

Table 5.1: Parameter estimation for the proposed model coefficients using algorithm(4.4).

	Max inductance point	Med inductance point	Min inductance point	Percent change
$\hat{R}_1$ [mΩ]	611.82	586.86	609.44	4.2
$\hat{R}_2$ [Ω]	653.31	688.25	713.67	8.4
$\hat{L}_1$ [μH]	379.73	347.27	304.50	21.4
$\hat{L}_2$ [μH]	1278.30	1208.93	1097.00	15.0

tion (4.2.1) of chapter (4) of this thesis. The model contains the estimated parameters: i.e., $\hat{R}_1$, $\hat{R}_2$, $\hat{L}_1$, and $\hat{L}_2$ for the maximum, medium and minimum inductance positions on rotor using Equations (4.1 to 4.4).

In this table, the model resistance (R_1 in $m\Omega$) remains constant with deviation of 4.2% for the maximum, medium, and minimum positions something similar to the Figure (5.1). This represents that R_1 does not change with respect to different rotor positions whereas R_2 varies in larger percentage,8.4%, as compare to R_1 as it represents the a part of core losses of the rotor and therefore varies more . However the series inductance L_1 in varies for different rotor position by 21.4% whereas L_2 varies with 15.0%. The both inductances L_1 and L_2 of the model show a larger magnitude at the measured maximum inductance position and smaller
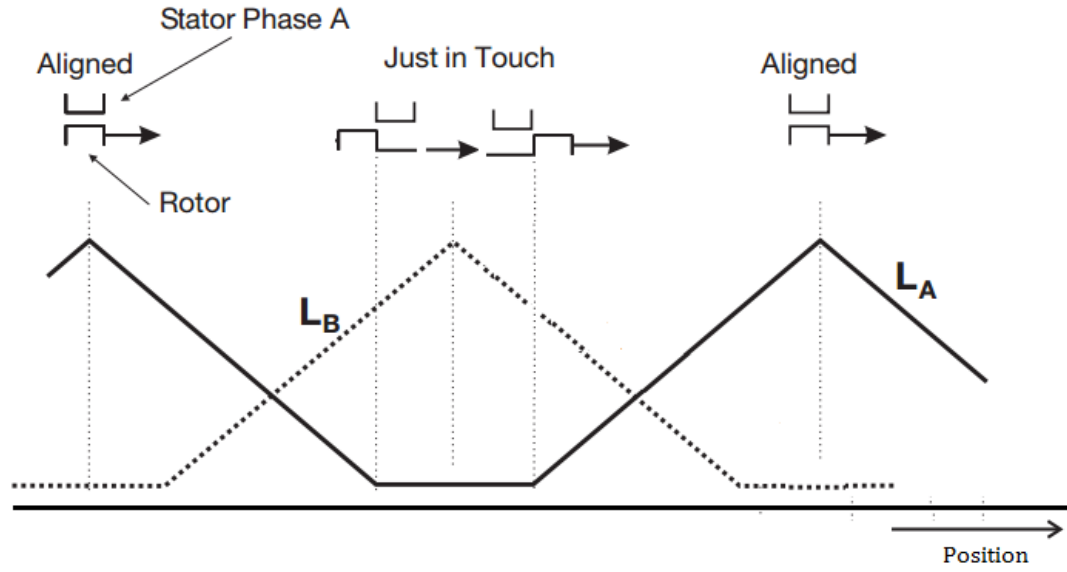
Figure 5.3: The different inductance rotor positions.

magnitude at minimum inductance position. Therefore, the inductance values at maximum position can be taken as direct inductance (L_{1d} and L_{1q}) and similarly for minimum point as quadrature inductance (L_{2d} and L_{2q}). The inductance is inversely proportional to reluctance and varies in motor per phase model accordingly.

The proposed model successfully depicts the actual motor per phase behaviour and also incorporates the direct and quadrature inductances information for different rotor positions. The rotor position can easily be monitored by examining the parameter variation of the model. This model is an advanced version of motor model that carries more information than a resistor in series with inductance model which has insufficient information regarding the variable inductance and reluctance phenomena of the permanent-magnet motors.

5.2 An On-line Motor Model Estimation Using IMP

In this section, a high frequency signal reconstruction has been obtained by adding a number of harmonics of a reference signal. Harmonics of the frequency of interest can be extracted by using the internal model principle. The main purpose of implementing internal model principle in our research is to extract harmonics for the BLDC motor's voltages and currents. Then calculating high energy harmonics' related magnitudes and phases. The on-line impedance of the motor can be determined using magnitude and phases of its harmonics. In order to estimate a model using IMP, we need to have an access to the neutral point of three phase motor, and an approximate model. Therefore, an on-line model estimation with IMP is beyond our thesis scope.

The Figures (5.4) and (5.5) are the implementation of IMP using thirty notch filters at the desired extraction of the harmonics. The notch filters are applied in the feedback of the estimation stabilizing tuning function L(s). For this part, the stall torque data has been used for the maximum, and minimum inductance rotor stall positions. The moment when motor is stalled, the applied the input voltages to the motor are completely consumed within the motor windings. Therefore, motor winding's impedance can be found by dividing the voltage dynamic function to the current transfer function i.e., $Z(s) = \frac{V(s)}{I(s)}$. The high frequency voltages (V_{AB}) are the three phase motor phase to phase voltages and currents are the phase current I_A and I_C. The motor phase voltage controller produces aperiodic high frequency signal as evident from estimator Figure (5.4), controller voltage frequency was slightly changed from 13 kHz.

At the same instant, the estimator took 0.5 ms to track the 13 kHz. The IMP model based Motor phase signal analysis is 8 time faster than Fast Fourier transform (FFT). We can not directly divide phase to phase voltages to the phase currents to get motor impedance. In order to apply IMP model, a dynamic motor model is required which is given in chapter (5). The stalling of the rotor position at the high inductance point and at minimum inductance point will provide different impedance for both the positions. The purpose of applying the internal model principle is to determine the frequency response of phase impedance model.
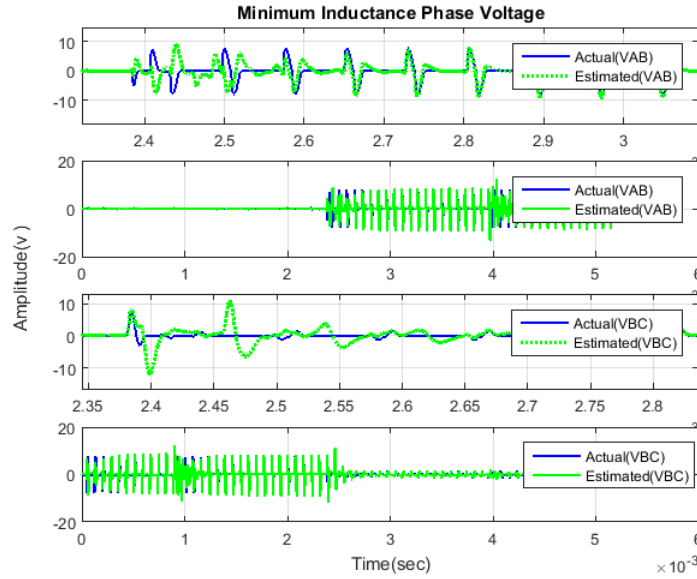
Figure 5.4: Motor Phase Voltage Estimation using (IMP algorithm).
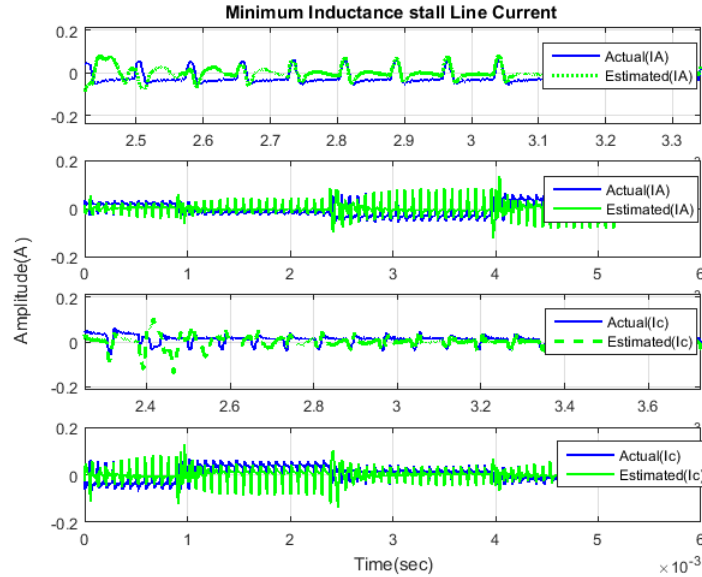

Figure 5.5: Motor Phase Current Estimation using (IMP algorithm).

The estimated IM model for each harmonic has two states x_1 and x_2 which are the trigonometric signals orthogonal to each other representing the components of real, and imag-

inary parts of the complex representation of the sinusoidal signals. All the harmonics are the complex model of the its component signals and obey all the complex number properties in signal processing.

The internal model for periodic and quasi-periodic signals can be implemented as single sinusoid models placed in parallel. Each IMP model is capable of exactly estimating the harmonic with exact energy and independent of the DC-off set decay for well modelled DC-offset.

5.2.1 An On-line Motor Model Estimation Using Extended EMF

This section presents the results of the implementation of an on-line sensorless rotor position identification technique i.e., the extended EMF. The motor parameters, such as stator resistance R_s, direct inductance L_d and quadrature inductance L_q, vary with load change on motor shaft. In this strategy, the parameters are modelled such that, the motor energy consuming and storing parameters do not affect the persistent estimation of position and it's speed. This model observer has been improved using a least quadratic regulator (LQR) as shown in Figure (5.6). The extended EMF observer response has considerably improved with LQR controller. The extended EMF model is parameter sensitive, there is a fair chance of it's going unstable, Therefore we need to be sure to have a better controller which can deals the parameters variation during on-line operation. Therefore, we require an observer that is stable as well as fast for an efficient sensorless rotor position identification. With the LQR based system gain tuning, the stability is guaranteed and therefore, we chose to improve the observer response with it and got improved results.

The Figure (5.7) represents the BLDC motor parameters such as phase to phase estimated resistance ($\hat{R}_s$), estimated direct inductance ($\hat{L}_d$) and estimated quadrature inductance ($\hat{L}_q$) using Equation (3.29). In this section, an off-line stator phase to phase resistance and inductance(i.e, L_d and L_q) is compared with the applied parameter identification used in [16]. The actual measured mean phase to phase stator resistance is $0.6\,\Omega$ *Appendix*(A.1, A.2 and A.3) at $100\,\text{Hz}$ using hand held LCR-meter (LCRModel879) for invariant rotor posi-
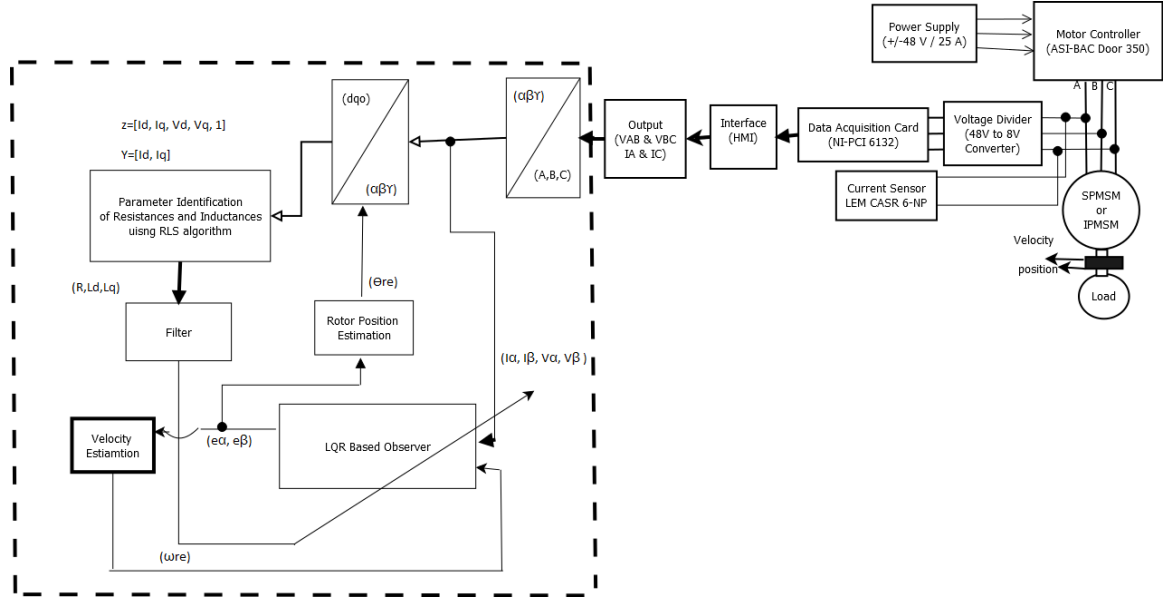
Figure 5.6: Proposed compensated LQR based observer and rotor position estimation strategy.

tion. However, Table(4.1) contains the measured phase to phase impedance values for various frequencies for maximum, intermediate and minimum inductance points on rotor. The phase to phase stator resistances and inductances are needed to be divided by 2 to get phase quantities. Therefore, **measured per phase parameters** are $R_s = 0.3\,\Omega$; $L_d = 1.8\,\text{mH}$; and $L_q = 1.5\,\text{mH}$, Whereas **the extended EMF** based estimated stator phase resistance $\hat{R}_s = 0.6$, direct and quadrature inductance $\hat{L}_d = 0.32\,\text{mH}$, and $L_q = 0.23\,\text{mH}$ can be seen in Figure(5.7) respectively. The reason of deviation, from actual to estimated values of resistances and inductances, is due to non-linearities, system chaotic behaviour, temperature, signal frequency, magnetic saturation, iron loses, which are not effective in off-line measurement. The current sensors (LEM CASR-NP6) was recorded using an additional wires with clamps to attach each phase to the Data acquisition card that could also be one of the reasons for stator resistance and inductance deviate.
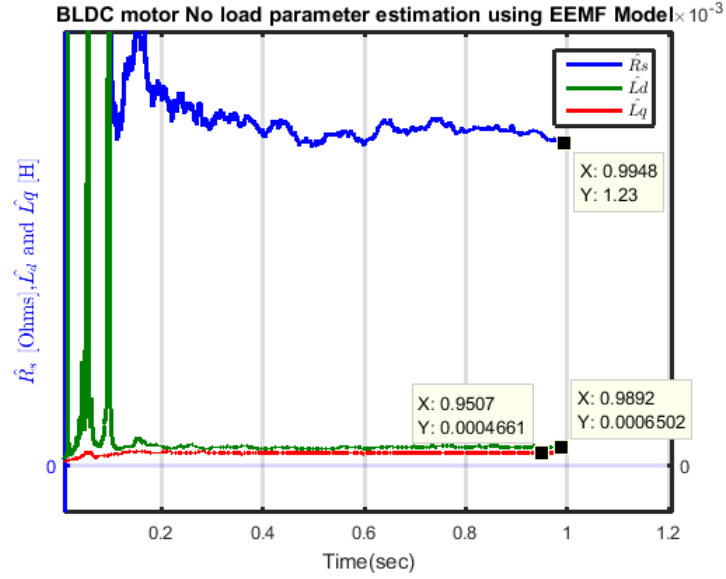
Figure 5.7: BLDC motor stator estimated resistance $\hat{R}_s$, and inductances $\hat{L}_d$ and $\hat{L}_q$ estimation using EEMF model at no load.

Table 5.2: Motor Parameters using Bac Door 350.

Rated Power	0.5 kW
Rated Current	73 A
DC Battery	±48 V
Reference Speed	5 Hz
pole pairs	23
Motor weight	12 kg
Magnetic field density (B)	0.58E+3 $\frac{Wb\cdot}{m^2}$
Inverter frequency	13 kHz
Sampling Rate	1 Sample$\cdot\mu$s^{-1}
EMF constant	0.038 $\frac{volt\cdot}{rad/s}$

5.2.2   Rotor Position Estimation via EEMF

the Figure (5.6) is the block diagram for the data acquisition set up for the motor under observation and also implementation of the extended EMF model with the improved observer

response using linear quadratic regulator (LQR) with better settling and response time. Since rotor position estimation without sensor may expected to behave lousy and unreliable therefore, the observer must be stable for a wide range of parameter change. Additionally, The estimation observer must act fast enough because we need rotor position for commutation process with negligible estimation error. The Figure(5.8) has been taken from [16] which
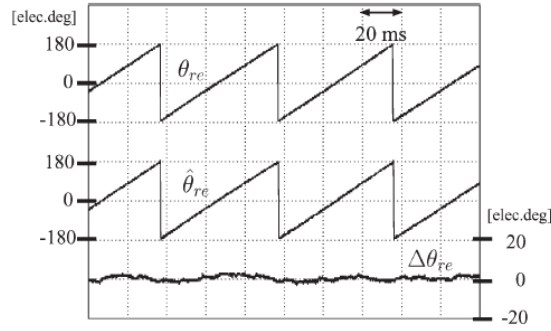
Figure 5.8: Extended EMF based rotor position estimation [16].

represents the position estimation in electrical degrees of the IPMSM rotating at 500 rpm. Where θ_{re} is the rotor position in electrical degrees $\hat{\theta}_{re}$ is the estimated rotor position.

$$\theta_e = \frac{P}{2} \times \theta_m \tag{5.1}$$

Therefore, the electrical degree estimation leads to mechanical angle (θ_m) rotor position measurement by the relationship between electrical and mechanical rotor position given by the Equation (5.1).

Figure 5.9: Fifth order Chebyshev(II), a lowpass filter with normalized cutoff frequency of 100 Hz to filter high frequency from motor voltages and stator current.

Figure 5.10: Extended EMF for the theoretical rotor position(θ_{re}).
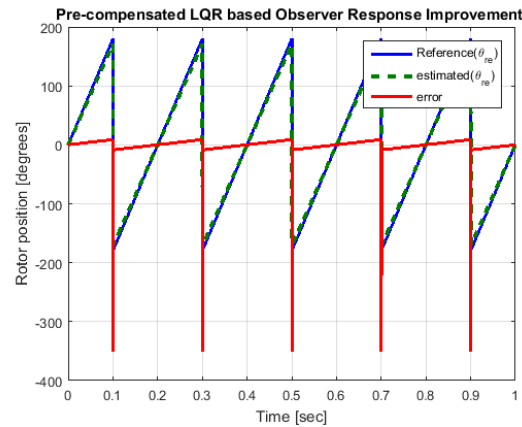
Figure 5.12: Pre-compensated LQR based extended EMF model observer improvement.
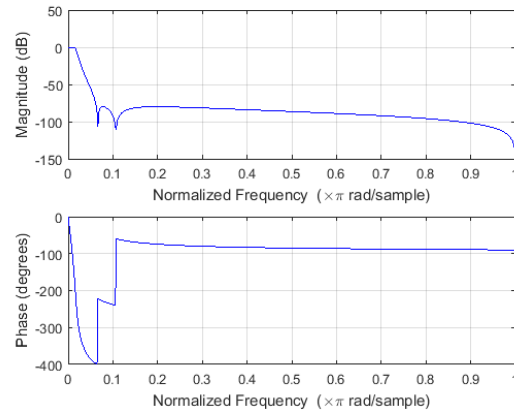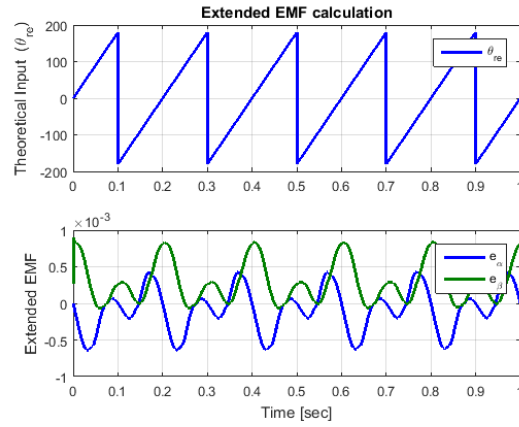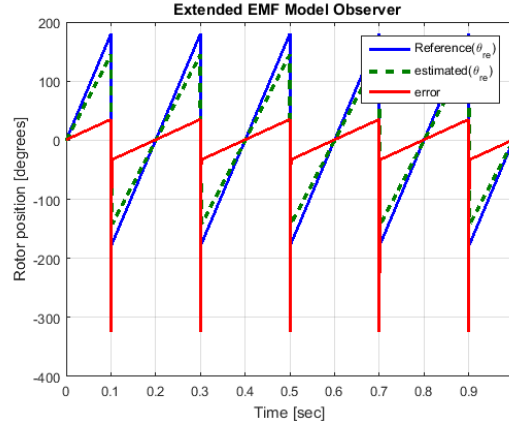
Figure 5.11: Applied Extended Model observer rotor position estimation.

The Figure(5.11) represents the extended EMF Model observer rotor position estimation where observer poles are given below.

$$poles = -1.8839 \pm j0.0111$$

The observer imitates the actual system and reduces the difference between the desired response to the estimated response. In control system a system design is based on rise time, settling time, and overshoot time. In his book, Chi-Tsong-chen, gives a detail difference between pole placement and linear quadratic regularization (LQR) method. The observer based on LQR, is preferred over pole placement due to stability concern of the controller. A LQR based controller can optimize the eigenvalues within the stable unit circle of stable region always meeting the design criterion. The matrices Q_c and R_c matrices in LQR state feedback gain controller method are the weight matrix. Their gain can be adjusted by trial and error. The benefit of LQR over pole placement method is the stability concern [4]. The poles of LQR based observer are at -1.1099e+04 and -2.8707e+03.

Figure 5.13: Pre-compensated LQR based extended EMF observer improvement.

5.3 Summary

In this chapter, a brief data description of the applied strategies,i.e., off-line motor model estimation using LMS, an on-line model estimation using IMP, 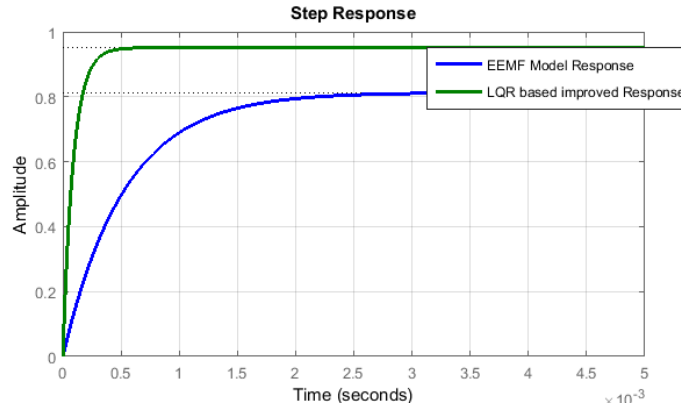and an on-line motor model based on extended EMF estimation. The main contribution of this thesis is a per phase BLDC motor impedance model. This model was presented by inspecting the frequency response of motor impedance response. Our motor phase dynamic impedance behaves like a resistor and inductor in series and as a resistor in parallel with the inductor. The parameters R_1, R_2, L_1 and L_2 have been estimated using least mean square. The proposed model data results were compared with the actual measured impedance point of three different inductance rotor positions. The proposed PMSM phase model is consistent with least error in resistance (R_1) in series and as well as in resistance (R_2) in parallel with inductance. The inductances, of the proposed motor per phase model, deviate more compare to the resistances. The frequency dependant inductance in this model is capable of actually imitating the real behaviour of permanent-magnet motor and can be used for a wide range of motor speed and rotary angle measurement.

Another contribution is the improvement in the extended EMF model observer response. The extended EMF is an on-line parameter identification strategy that can estimate the motor

angular velocity, and rotor position using identification theory. The velocity and rotor position are recursively updated in the motor model. The observer response has been improved by using a compensated LQR estimator in order to reduce error system error and making motor independent of load variation. As in the process of commutation it is better to have better estimation results compare to rotor mounted rotor position sensors.

Chapter 6

Conclusion and Future Work

6.1 Conclusion

- In this thesis, an extended EMF model has been applied on a motor under observation with unknown parameters. An on-line parameter identification observer with minimum order estimates the motor angular velocity, and rotor position. The velocity and rotor position are cursively updated in the motor model. The Observer response has been improved by using a compensated LQR estimator in order to reduce system error and making motor independent of load variation. In the process of commutation it is recommended to have better estimation results compare to rotor mounted rotor position sensors. Because here we are intending to replace rotor position sensors with an estimate of it using motor energizing signals.

- A per phase BLDC motor impedance model has been proposed by inspecting the frequency response of motor impedance response. Our motor phase dynamic impedance behaves like a resistor and inductor in series and iron losses are represented as a resistor in parallel with the inductor. Parameters R_1, R_2, L_1 and L_2 have been estimated using an estimation technique: the least mean square (LMS). The proposed PMSM phase model is consistent with least error in resistance (R_1) in series and as well as in resistance (R_2) in parallel with inductance. The inductance, of the proposed motor per phase model, deviates more compare to the resistance in series. The frequency dependant inductance in this model is capable of actually imitating

the real behaviour of permanent-magnet motor and can be used for a wide range of motor speed and rotary angle measurement.

- The internal model principle algorithm based motor dynamic model has been estimated which given in chapter 4 of this thesis. Internal model is an efficient way of determining dynamic system equivalent models with the help of input/output signals harmonics and a possible equivalent system model e.g, Irshad Mohsin and L.J.Brown (2012) estimated an equivalent dynamic model of (Resistance spot welding) RSW process [31].

- As most of the phase winding are modelled the same way a resistor in series with an inductor, ignoring the fact that inductance is a function of rotor position and changes due to changing air gap between the rotor and stator. That's the reason we proposed the dynamic impedance model for our motor. Frequency response of this model is well matching the actual impedance points therefore replacing series phase model in Extended EMF with this model will be able to respond both in lower and high frequencies considering the non-linearities of the system as well.

6.2 Future Work Recommendations

- So far the existing sensorless rotor position estimation techniques have not been tested in extreme environmental conditions. A comparative study of sensor-based and sensorless techniques should be undertaken to compare the performance and reliability of the single salient and double salient synchronous motors by varying the external parameters such as sensorless motor speed control in automated drilling rigs etc.

- The model phase impedance may be replaced in with series resistance with inductance model. In order to bring non-linearities of the system in account.

- In future, for better speed control and parameter identification "**Gain Scheduled Model predictive control**" (MPC) should be applied using our proposed per phase motor model for reliable model performance.

– A comparative study can be conducted by replacing the extended EMF estimation system by Kalman filter based parameter estimation.

Bibliography

[1] S. Rajakaruna, F. Shahnia, and A. Ghosh, "Plug in electric vehicles in smart grids," 2015.

[2] T. Kato, K. Akatsu, T. Shigeta, M. Nakano, M. Tsukamoto, and M. Arimitsu, "Principle of a variable characteristic motor with compound magnetomotive forces," in *Power Electronics Conference (IPEC), 2010 International*, pp. 1969–1974, June 2010.

[3] M. Ikhlas, *"Rotor Position Identification for Brushless DC motor (2015).", University of Western Ontario - Electronic Thesis and Dissertation Repository. Paper 2676. http://ir.lib.uwo.ca/etd/2676.* 2015.

[4] C.-T. Chen, *"Linear system theory and design.", 3rd ed. New York: Oxford University Press.* Oxford University press 1999.

[5] J. Fang, *"The LQR controller design of two-wheeled self-balancing robot based on the particle swarm optimization algorithm.".*

[6] T.A.Lipo, *"Analysis of Synchronous Machines",2nd Edition, CRC press June 25,2012.* CRC Press Taylor and Francis group.

[7] R. Krishnan, S.-Y. Park, and K. Ha, "Theory and operation of a four-quadrant switched reluctance motor drive with a single controllable switch-the lowest cost four-quadrant brushless motor drive," *Industry Applications, IEEE Transactions on*, vol. 41, pp. 1047–1055, July 2005.

[8] R.Krishnan, *" Switched reluctance motor drives: Modeling, simulation, analysis, design and applications(2001).", Boca Raton, Fla; London: CRC Press.* 2001.

[9] *"http://www.ti.com/lit/an/spra420a/spra420a.pdf "*. Texas Instruments.

[10] B. Fahimi, A. Emadi, and R. Sepe, "Position sensorless control," *Industry Applications Magazine, IEEE*, vol. 10, pp. 40–47, Jan 2004.

[11] X. Liu, Z. Zhu, M. Hasegawa, A. Pride, R. Deodhar, T. Maruyama, and Z. Chen, "Performance comparison between unipolar and bipolar excitations in switched reluctance machine with sinusoidal and rectangular waveforms," in *Energy Conversion Congress and Exposition (ECCE), 2011 IEEE*, pp. 1590–1595, Sept 2011.

[12] N. Nakao and K. Akatsu, "Vector control specialized for switched reluctance motor drives," in *Electrical Machines (ICEM), 2014 International Conference on*, pp. 943–949, Sept 2014.

[13] R. Hoseinnezhad, A. Bab-Hadiashar, and P. Harding, "Calibration of resolver sensors in electromechanical braking systems: A modified recursive weighted least-squares approach," *Industrial Electronics, IEEE Transactions on*, vol. 54, pp. 1052–1060, April 2007.

[14] G. Brasseur, "Robust automotive sensors," in *Instrumentation and Measurement Technology Conference, 1997. IMTC/97. Proceedings. Sensing, Processing, Networking., IEEE*, vol. 2, pp. 1278–1283 vol.2, May 1997.

[15] B. Fahimi, A. Emadi, and J. Sepe, R.B., "Four-quadrant position sensorless control in srm drives over the entire speed range," *Power Electronics, IEEE Transactions on*, vol. 20, pp. 154–163, Jan 2005.

[16] S. Ichikawa, M. Tomita, S. Doki, and S. Okuma, "Sensorless control of permanent-magnet synchronous motors using online parameter identification based on system iden-

tification theory," *Industrial Electronics, IEEE Transactions on*, vol. 53, pp. 363–372, April 2006.

[17] J. Cai and Z. Deng, "Sensorless control of switched reluctance motor based on phase inductance vectors," *Power Electronics, IEEE Transactions on*, vol. 27, pp. 3410–3423, July 2012.

[18] D. Torrey, "Switched reluctance generators and their control," *Industrial Electronics, IEEE Transactions on*, vol. 49, pp. 3–14, Feb 2002.

[19] A. Kawamura, "Survey of position sensorless switched reluctance motor control," in *Industrial Electronics, Control and Instrumentation, 1994. IECON '94., 20th International Conference on*, vol. 3, pp. 1595–1598 vol.3, Sep 1994.

[20] K. Hwu and C. Liaw, "Intelligent tuning of commutation for maximum torque capability of a switched reluctance motor," *Energy Conversion, IEEE Transactions on*, vol. 18, pp. 113–120, Mar 2003.

[21] Z. Zhu and D. Howe, "Electrical machines and drives for electric, hybrid, and fuel cell vehicles," *Proceedings of the IEEE*, vol. 95, pp. 746–765, April 2007.

[22] G. Jang, J. Park, and J. Chang, "Position detection and start-up algorithm of a rotor in a sensorless bldc motor utilising inductance variation," *Electric Power Applications, IEE Proceedings -*, vol. 149, pp. 137–142, Mar 2002.

[23] M. Boussak, "Sensorless speed control and initial rotor position estimation of an interior permanent magnet synchronous motor drive," in *IECON 02 [Industrial Electronics Society, IEEE 2002 28th Annual Conference of the]*, vol. 1, pp. 662–667 vol.1, Nov 2002.

[24] M. Ying and P. Zaiping, "A novel starting method of sensorless bldc motors for electric vehicles," in *Electrical and Control Engineering (ICECE), 2010 International Conference on*, pp. 3212–3215, June 2010.

[25] R. Miller and M. R.Miller, *" Electric motors.", All new 6th ed. Indianapolis, Ind: Wiley publisher*. Wiley publisher, 2004.

[26] *"Heaviside O., Electrical Papers, Vol 2L.; N.Y.: Macmillan, 1892, p.166"*. Macmillan.

[27] R. Krishnan, *"Permanent magnet synchronous and brushless DC motor drives.", 1st ed. Boca Raton: CRC Press/Taylor Francis.* CRC/Taylor Francis, 2010.

[28] *"http://www.ni.com/pdf/products/us/043918301101dlr.pdf"*.

[29] *"http://www.digikey.ca/Web%20Export/Supplier%20Content/LEM398/PDF"*. DigiKey.

[30] B. A. Francis and W. M. Wonham, "The internal model principle of control theory," *Automatica*, vol. 12, no. 5, pp. 457–465, 1976.

[31] M. M. Irshad, *" Technique for measurement of weld resistance for AC resistance spot welding via instantaneous phasor measurement.", Ph.D. diss., School of Graduate and Postdoctoral Studies, University of Western Ontario.* 2012.

[32] S. Morimoto, K. Kawamoto, M. Sanada, and Y. Takeda, "Sensorless control strategy for salient-pole pmsm based on extended emf in rotating reference frame," in *Industry Applications Conference, 2001. Thirty-Sixth IAS Annual Meeting. Conference Record of the 2001 IEEE*, vol. 4, pp. 2637–2644 vol.4, Sept 2001.

Appendix A

Impedence Measurement for BLDC motors

Table A.1: Phase AB Impedance Measurement

Frequency kHz	$R_s\,\Omega$	$R_p\,\Omega$	$L_s\,$mH	$L_p\,$mH	$\angle\theta_{ab}$
0.1	0.6	2.6	1.73	2.28	$\angle 60.5°$
1	0.88	116.58	1.7	1.71	$\angle 84.8°$
10	19.26	451.8	1.51	1.58	$\angle 78.2°$

Table A.2: Phase BC Impedance Measurement

Frequency kHz	$R_s\,\Omega$	$R_p\,\Omega$	$L_s\,$mH	$L_p\,$mH	$\angle\theta_{bc}$
0.1	0.6	1.86	1.38	2.04	$\angle 55.6°$
1	0.88	84.28	1.36	1.37	$\angle 84.2°$
10	13.48	422.4	1.23	1.27	$\angle 79.7°$

Table A.3: Phase CA Impedance Measurement

Frequency kHz	$R_s\,\Omega$	$R_p\,\Omega$	$L_s\,$mH	$L_p\,$mH	$\angle\theta_{ca}$
0.1	0.62	2.2	1.56	2.16	$\angle 59°$
1	0.9	104	1.546	1.5602	$\angle 84.6°$
10	16.44	446.5	1.394.3	1.4476	$\angle 79°$

Appendix B

Theoretical Inductance for Balanced Case

B.1 Three Phase Inductance

Equations(B.1, B.2 and B.3) are the three inductances for balanced case. We need to find the angle at what inductance values maximum and what angles we see the the minimum values.Where L_{base} is the reference inductance and L_{dev} is the deviation in the inductance.

$$L_{ab} = 2L_{base} + L_{dev}cos(\theta_m) + L_{dev}cos(\theta_m - \frac{2\pi}{3}) \tag{B.1}$$

$$L_{bc} = 2L_{base} + L_{dev}cos(\theta_m + \frac{2\pi}{3}) + L_{dev}cos(\theta_m - \frac{2\pi}{3}) \tag{B.2}$$

$$L_{ca} = 2L_{base} + L_{dev}cos(\theta_m) + L_{dev}cos(\theta_m + \frac{2\pi}{3}) \tag{B.3}$$

- **Equation(B.1):**

  * **Domain**: $[0 \leq \theta_m \leq 2\pi l]$ For $l = \pm 0, 1, 2, 3, \ldots$
  * **Stationary Points/ Critical Points:** $\theta_m = \frac{2\pi}{3}$ and $\frac{5\pi}{3}$
  * **Local Maxima** of L_{ab} is $(\frac{5\pi}{3}, m)$ and **Local Minima** is $(\frac{2\pi}{3}, n)$ where, $m > n$.

- **Equation(B.2):**

  * **Domain:** $[0 \leq \theta_m \leq 2\pi l]$, For $l = \pm 0, 1, 2, 3, \ldots$

∗ **Stationary Points/ Critical Points:** $\theta_m = 0$, π and 2π

∗ **Local Maxima** of L_{bc} is (π, m) and **Local Minima** points are $(0,\ n)$ and $(2\pi,\ n)$ where, $m\ >\ n$.

– **Equation(B.3):**

∗ **Domain** $[0 \leq \theta_m \leq 2\pi l]$, For $l = \pm 0, 1, 2, 3, \ldots$

∗ **Stationary Points/ Critical Points:** $\theta_m = \frac{\pi}{3}$ and $\frac{4\pi}{3}$

∗ Local Maxima of L_{ca} is $(\frac{\pi}{3}, m)$ and Local Minima points are $(\frac{4\pi}{3}, n)$ where, $m > n$.

Curriculum Vitae

Name:	Iram Raza
Post-Secondary Education and Degrees:	Mehran University of Engineering and Technology, Pakistan 2004-2008 B.Eng. Electrical Engineering Western Univesity London, Ontario, Canada 2013 - 2016 M.E.Sc. Electrical Engineering
Related Work Experience:	Research/Teaching Assistant Western University London, Ontario, Canada 2013 - 2016 Teaching Assistant(Electrical Deapartment) Balochistan University of Information technology, engineering and management sciences(BUITEMS) Quetta, Pakistan 2012-2013